Vol. 88 No. 1 pp. 176–195 ACTA GEOLOGICA SINICA (English Edition) Feb. 2014

Trace Element Geochemistry of Magnetite from the Fe(-Cu) Deposits in the Hami Region, Eastern Tianshan Orogenic Belt, NW China

HUANG Xiaowen[1, 2], QI Liang[1, *] and MENG Yumiao[1, 2]

1 *State Key Laboratory of Ore Deposit Geochemistry, Institute of Geochemistry, Chinese Academy of Sciences, Guiyang 550002, Guizhou, China*

2 *University of Chinese Academy of Sciences, Beijing 100049, China*

Abstract: Laser ablation–inductively coupled plasma–mass spectrometry (LA–ICP–MS) was used to determine the trace element concentrations of magnetite from the Heifengshan, Shuangfengshan, and Shaquanzi Fe(–Cu) deposits in the Eastern Tianshan Orogenic Belt. The magnetite from these deposits typically contains detectable Mg, Al, Ti, V, Cr, Mn, Co, Ni, Zn and Ga. The trace element contents in magnetite generally vary less than one order of magnitude. The subtle variations of trace element concentrations within a magnetite grain and between the magnetite grains in the same sample probably indicate local inhomogeneity of ore–forming fluids. The variations of Co in magnetite between samples are probably due to the mineral proportion of magnetite and pyrite. Factor analysis has discriminated three types of magnetite: Ni–Mn–V–Ti (Factor 1), Mg–Al–Zn (Factor 2), and Ga–Co (Factor 3) magnetite. Magnetite from the Heifengshan and Shuangfengshan Fe deposits has similar normalized trace element spider patterns and cannot be discriminated according to these factors. However, magnetite from the Shaquanzi Fe–Cu deposit has affinity to Factor 2 with lower Mg and Al but higher Zn concentrations, indicating that the ore–forming fluids responsible for the Fe–Cu deposit are different from those for Fe deposits. Chemical composition of magnetite indicates that magnetite from these Fe(–Cu) deposits was formed by hydrothermal processes rather than magmatic differentiation. The formation of these Fe(–Cu) deposits may be related to felsic magmatism.

Key words: trace elements, magnetite, LA–ICP–MS, Fe(–Cu) deposits, Eastern Tianshan Orogenic Belt, Xinjiang

1 Introduction

Magnetite commonly occurs as an accessory mineral in igneous, metamorphic and sedimentary rocks, and can be major to trace minerals in various types of mineral deposits. Magnetite can incorporate various amounts and assemblages of trace elements in its spinel structure during formation in various ore–forming environments, and hence the compositional variety can be used to fingerprint mineralization types and discriminate geochemical vectors (Carew, 2004; Carew et al., 2006; Singoyi et al., 2006; Beaudoin and Dupuis, 2009; Rusk et al., 2009; Dupuis and Beaudoin, 2011; Zhang et al., 2011; Berzina, 2012; Nadoll et al., 2012).

Many geochemical studies of magnetite have focused on igneous systems because numerous experimental data are available about the partition coefficients of trace elements between magnetite and silicate melts (Dare et al., 2012 and references therein). The compositional variations in Fe–Ti oxides can be used to identify or correlate different stages of eruptive events (Shane, 1998) and the variations of V and Ti contents can indicate the changes of temperature and oxygen fugacity (Frost, 1991; Nielsen et al., 1994; Devine et al., 2003; Ryabchikov and Kogarko, 2006; Turner et al., 2008). In addition, Fe–oxide geochemistry is also a sensitive petrogenetic indicator for the degree of sulfide fractionation and can be used for provenance discrimination (Dare et al., 2012).

Compared to the studies of igneous magnetite, the geochemistry of hydrothermal magnetite has not been extensively studied because of the limited thermodynamic data and the low-level trace elements. The trace elements of hydrothermal–related magnetite have been investigated using a variety of analytical techniques. The solution ICP–MS technology was used to determine the trace element

* Corresponding author. E-mail: qilianghku@hotmail.com

contents of magnetite from the Osborne Cu–Au deposit and Kiruna–type iron deposits of Sweden and Chile (Nystroem and Henriquez, 1994; Banvill, 1998). Variations of V and Cr in magnetite were explained to different ore–forming stages or processes. However, possible impurity of magnetite during mineral separation restricts the application of this technique. The development of the laser ablation (LA)–ICP–MS technique for magnetite (Norman et al., 1996; Liu et al., 2008; Nadoll and Koenig, 2011; Zhang et al., 2012) has the advantages of the solution ICP–MS technique and further provides in situ analyses of trace elements in magnetite. Due to the very low detection limits (as low as 0.00x ppm) afforded by LA–ICP–MS, the nature and distribution of major and trace elements in magnetite can be simultaneously assessed. Moreover, less element fractionation during ablation and transport indicates that the technique of laser ablation can provide homogeneous concentrations of trace elements in a single magnetite grain (Müller et al., 2003). The subtle variations of trace element contents can be used to discriminate magnetite from different geologic settings (Singoyi et al., 2006; Nadoll et al., 2012).

The Eastern Tianshan Orogenic Belt (ETOB) has been an important target for mineral exploration in China (Wang et al., 2006a; Zhang et al., 2006; Mao et al., 2012). Numerous Fe(–Cu) deposits including the Yamansu, Heifengshan, Shuangfengshan, and Shaquanzi Fe(–Cu) deposits in the Hami region constitute the Aqishan–Yamansu metallogenic belt (Gao et al., 1993; Che et al., 1994; Hua, 2001; Hua et al., 2002; Qin et al., 2002; Wang et al., 2006a). These Fe(–Cu) deposits have been described mainly in Chinese literatures (Song et al., 1983; He et al., 1994a; Jiang et al., 2002; Xiao, 2003; Fang et al., 2006a, 2006b; Huang et al., 2013a). However, their origins are poorly understood.

In this study, we show detailed trace element compositions of magnetite from the Heifengshan, Shuangfengshan, and Shaquanzi Fe(–Cu) deposits. The trace element data measured by LA–ICP–MS combined with factor analysis are used to characterize and discriminate magnetite from the three ore–forming systems and constrain the origin of these Fe(–Cu) deposits.

2 Geological Setting

The ETOB is bounded by the Xiaorequanzi to the west and the junction of Gansu Province and Xinjiang Uygur Autonomous Region to the east, covering an area of about 60,000 km^2 (Fig. 1). The ETOB is mainly composed of four tectonic units from north to south, including the Dananhu–Tousuquan arc belt, the Kanggurtag belt, the Aqishan–Yamansu belt, and the Central Tianshan belt (He et al., 1994b; Gao et al., 1998; Qin et al., 2002, 2003; Xiao et al., 2004; Wang et al., 2006a, 2006b; Qi et al., 2008; Charvet et al., 2011) (Fig. 1). These belts are separated by several approximately east–west–trending faults (Fig. 1).

The Dananhu–Tousuquan arc belt is made up of the Devonian to Carboniferous island arc volcanic rocks (Mao et al., 2005). In the Kanggurtag belt, there are mylonite, tectonic lenses, and breccias formed along early extensional faults (Qin et al., 2002; Xu et al., 2003). The Carboniferous strata of the Kanggurtag belt are composed of fine–grained sandstone and carbonaceous argillite. The Aqishan–Yamansu belt is bounded to the north by the Kushui fault from the Kanggurtag belt and to the south by the Shaquanzi fault. The Aqishan–Yamansu belt comprises a 5 km thick succession of the lower Carboniferous Yamansu Formation of bimodal volcanic rocks, the middle Carboniferous Shaquanzi Formation of clastic rocks and andesitic tuff, and the upper Carboniferous Tugutublak Formation of intercalated carbonate. The Permian marine and terrestrial clastic rocks are intercalated with bimodal volcanic rocks and carbonates (Mao et al., 2005). The Central Tianshan belt in Eastern Tianshan has been regarded as a composite volcanic arc, which is composed of Precambrian basement rocks of amphibolite facies, overlain by calc–alkaline basaltic andesite, volcanoclastics, minor I–type granite and granodiorite (Xiao et al., 2004; Liu et al., 2004; Hu et al., 2007; Shi et al., 2007). The Precambrian basement consists of gneiss, quartz schist, migmatite and marble.

The study area, located in the eastern part of the Aqishan–Yamansu belt, is an important cluster of Fe(–Cu) deposits, including the Heifengshan, Shuangfengshan, Shaquanzi deposits and some Fe ore occurrences (Fig. 2). The strata at this area include the Proterozoic central Tianshan Group, early Carboniferous Yamansu and Dikan'er Formations, early Permian Aqikebulak Formation and Cenozoic rocks. The Yamansu Formation is composed of bimodal volcanic and clastic rocks, including andesitic tuff, andesitic tuff breccia, limestone, potash–keratophyre and felsic porphyry (Yang et al., 1996; Hou et al., 2006). The Dikan'er Formation consists of intermediate–mafic volcanic rocks, clastic rocks and carbonate rocks, which has a zircon U–Pb age of ~320 Ma (Li et al., 2011). The Aqikebulak Formation consists of basaltic to rhyolitic rocks and sandstone. Carboniferous intrusions are widespread at the Shaquanzi area, including granite, diorite, and granodiorite.

The Heifengshan, Shuangfengshan and Shaquanzi Fe(–Cu) deposits share similar geological and mineralization features. Both the Heifengshan and Shuangfengshan Fe deposits contain Fe–rich ores with an average ore grade of 44 wt.% Fe (Huang et al., 2013a), whereas the Shaquanzi Fe–Cu deposit contains Fe–Cu ores with grades of 25–36

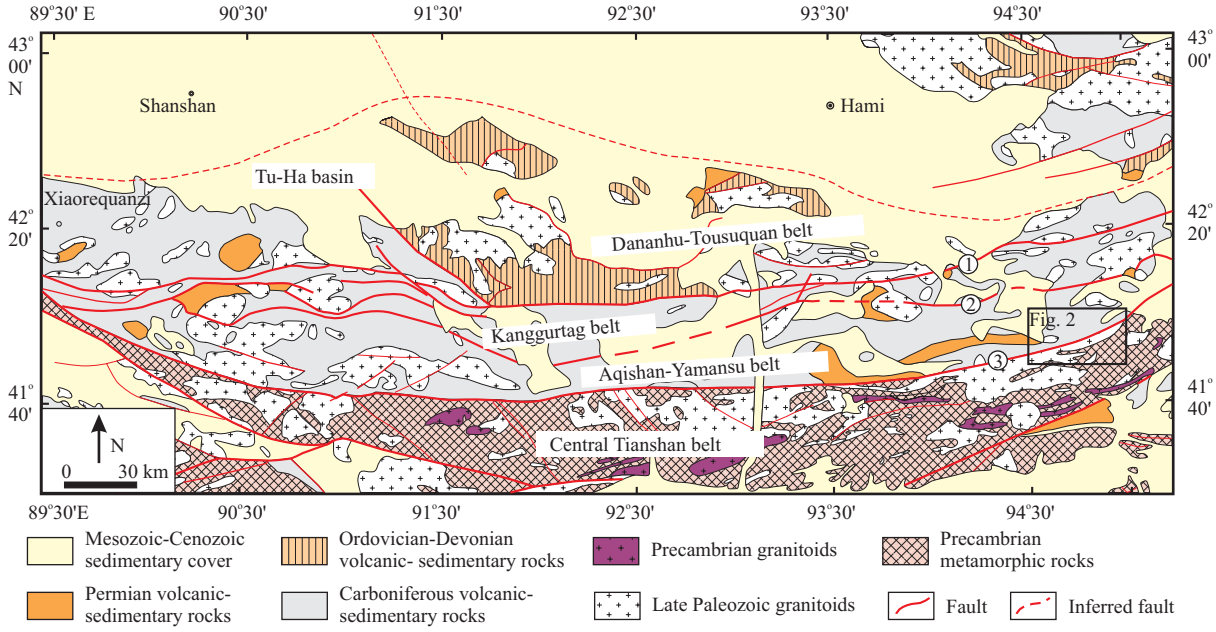

Fig. 1. A simplified geological map of Eastern Tianshan Orogenic Beltu[1].
Faults: ①–Kanggur fault; ②–Kushui fault; ③–Shaquanzi fault

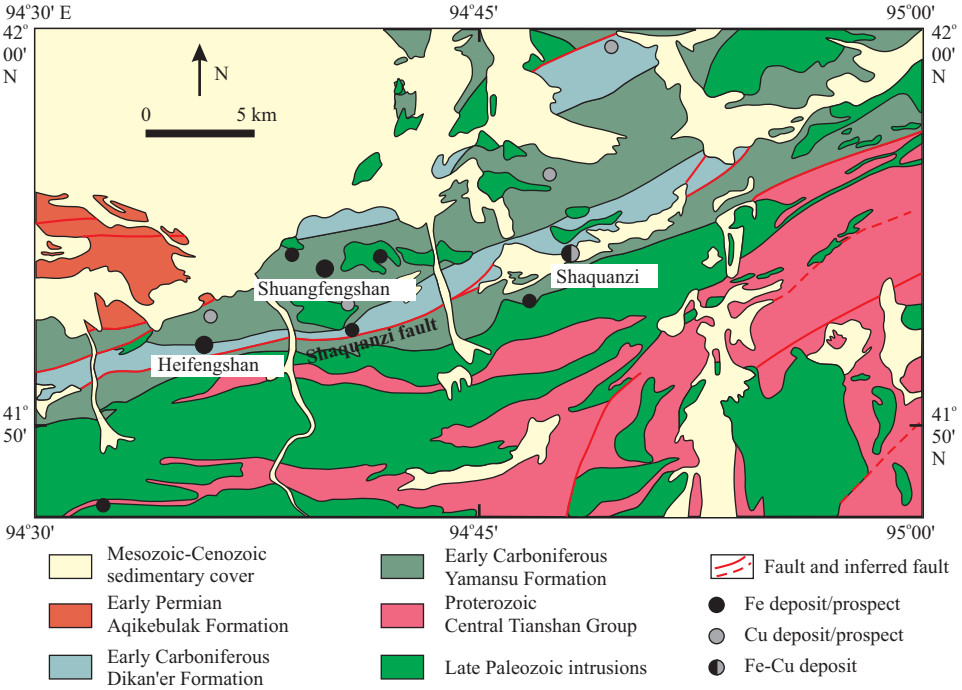

Fig. 2. A sketch geological map of the Shaquanzi area[2].

wt.% Fe and 0.5–2.3 wt.% Cu (Zeng, 1962; Fang et al., 2006a). Both the Heifengshan Fe deposit and Shaquanzi Fe–Cu deposit are hosted in the early Carboniferous Dikan'er Formation, whereas the Shuangfengshan Fe deposit is hosted in the early Carboniferous Yamansu Formation. These deposits are composed of vein–type and lens–shaped ore bodies hosted in the transitional zone between volcanic and sedimentary rocks. The country rocks are locally intruded by dioritic dikes, leading to the formation of epidote skarn (Jiang et al., 2002). Extensive hydrothermal alteration in these deposits includes chloritization, epidotization, carbonation, pyritization and albitization. Metallic minerals are magnetite, pyrite and minor chalcopyrite, whereas gangue minerals include chlorite, epidote, calcite and quartz.

3 Ore Petrography

3.1 Heifengshan Fe deposit

Magnetite grains from two types of ores, massive

(HFS0901, HFS0904 and HFS0910) and disseminated ores (HFS0903 and HFS0906), are chosen for trace element analyses in the Heifengshan Fe deposit (Fig. 3a–c). Both types of ores have similar mineral assemblages of magnetite, pyrite, calcite and minor chlorite. Magnetite grains from the massive ores occur as anhedral to euhedral crystals that are typically smaller than 200 μm in diameter (Fig. 4a). However, magnetite around calcite clots generally has larger grain sizes (up to several mm across) than those away from calcite (Fig. 4b). Disseminated ores have magnetite disseminated in the volcanic rocks or growing along the boundary of calcite or pyrite (Fig. 3b). Magnetite grains from the disseminated ores generally occur as anhedral to euhedral crystals that are smaller than 100 μm across.

3.2 Shuangfengshan Fe deposit

Similar to the Heifengshan Fe deposit, the Shuangfengshan Fe deposit is also composed of massive and disseminated ores (Fig. 3d–f). Magnetite is commonly associated with pyrite and calcite. Euhedral pyrite is typically disseminated in the calcite clots of the massive ores (Fig. 3d). Disseminated ores are commonly composed of fine–grained magnetite and anhedral to euhedral pyrite (Fig. 3e). Locally, euhedral pyrite is particularly developed, forming the massive sulfide ores (Fig. 3f). Magnetite from the massive ores commonly has platy crystals that have a length of ~200 μm and a width of ~60 μm (Fig. 4c). Petrographic observations show that straight contacts and absence of reaction boundaries between magnetite and other minerals such as pyrite and calcite in the Shuangfengshan Fe deposit (Fig. 4d), indicating that magnetite was in equilibrium with accompanying phases such as pyrite and calcite.

3.3 Shaquanzi Fe–Cu deposit

Massive ores are dominant in the Shaquanzi Fe–Cu deposit, which are composed of magnetite, pyrite, chalcopyrite and calcite (Fig. 3g–h). Magnetite commonly occurs as anhedral crystals and pyrite infills the fracture of magnetite (Fig. 4e). Magnetite also occurs as columnar or radial crystals that are less than 200 μm across and is locally infilled by pyrite (Fig. 4f).

4 Analytical Methods

4.1 Chemical compositions of magnetite

Major and trace elements of magnetite were determined by a Coherent GeoLasPro 193 nm LA system coupled with an Agilent 7700x ICP–MS at the State Key Lab of Ore Deposit Geochemistry, Institute of Geochemistry, Chinese Academy of Sciences. A total of 37 elements were analyzed using isotopes ^{23}Na, ^{25}Mg, ^{27}Al, ^{29}Si, ^{31}P, ^{39}K, ^{44}Ca, ^{45}Sc, ^{49}Ti, ^{51}V, ^{53}Cr, ^{55}Mn, ^{57}Fe, ^{59}Co, ^{60}Ni, ^{65}Cu, ^{66}Zn, ^{71}Ga, ^{74}Ge, ^{85}Rb, ^{88}Sr, ^{89}Y, ^{90}Zr, ^{93}Nb, ^{95}Mo, ^{107}Ag, ^{111}Cd, ^{115}In, ^{118}Sn, ^{137}Ba, ^{178}Hf, ^{181}Ta, ^{182}W, ^{208}Pb, ^{209}Bi, ^{232}Th and ^{238}U. Detailed operating conditions for the laser ablation system and the ICP–MS instrument and data reduction are similar as described by Liu et al. (2008). Helium was applied as a carrier gas, and argon was used as the make–up gas and mixed with the carrier gas via a T–connector before entering the ICP. Each analysis incorporated a background acquisition of approximately 20 s (gas blank) followed by 40 s data acquisition from the sample. Analytical spots (44 or 60 μm) were ablated by 160 successive laser pulses (4 Hz). Element contents were calibrated against multiple–reference materials (GSE–1G, BCR–2G, BIR–1G, BHVO–2G and NIST610) using ^{57}Fe as internal standard (Liu et al., 2008). Every 8 sample analyses were followed by one analysis of GSE–1G as quantity control to correct the time–dependent drift of sensitivity and mass discrimination. Off–line selection and integration of background and analyte signals, and time–drift correction and quantitative calibration were performed by ICPMSDataCal (Liu et al., 2008).

4.2 The principle of factor analysis

Factor analysis is a powerful statistical method for examining underlying relations among the trace element compositions of magnetite. Factor analysis was performed by the statistical package SPSS Version 18 using a principal component extraction method with a Kaiser Varimax rotation (Kaiser, 1958) and a Bartlett factor score. Rotated solutions can describe the most important interrelations in a dataset more directly than the unrotated solutions (Kaiser, 1958; Cliff and Krus, 1976) and maximize the variance of the factor loadings by adjusting them to be either near ±1 or near zero (Davis, 1986). Factor scores for each individual analysis are derived from the factor loadings and represent the significance of a given factor for a specific sample or analysis. Factor scores >1 indicate a high significance of the given factor, whereas negative values (<–1) indicate the given factor has no significance. As pointed out by Nadoll et al. (2012), only factor scores that lie outside the –0.5 to 0.5 intervals would be meaningful for the data assessment.

5 Analytical Results

5.1 Magnetite geochemistry

LA–ICP–MS data show that magnetite grains from the Heifengshan, Shuangfengshan, and Shaquanzi Fe(–Cu) deposits have similar trace element contents but show characteristic variations of specific elements. Magnesium,

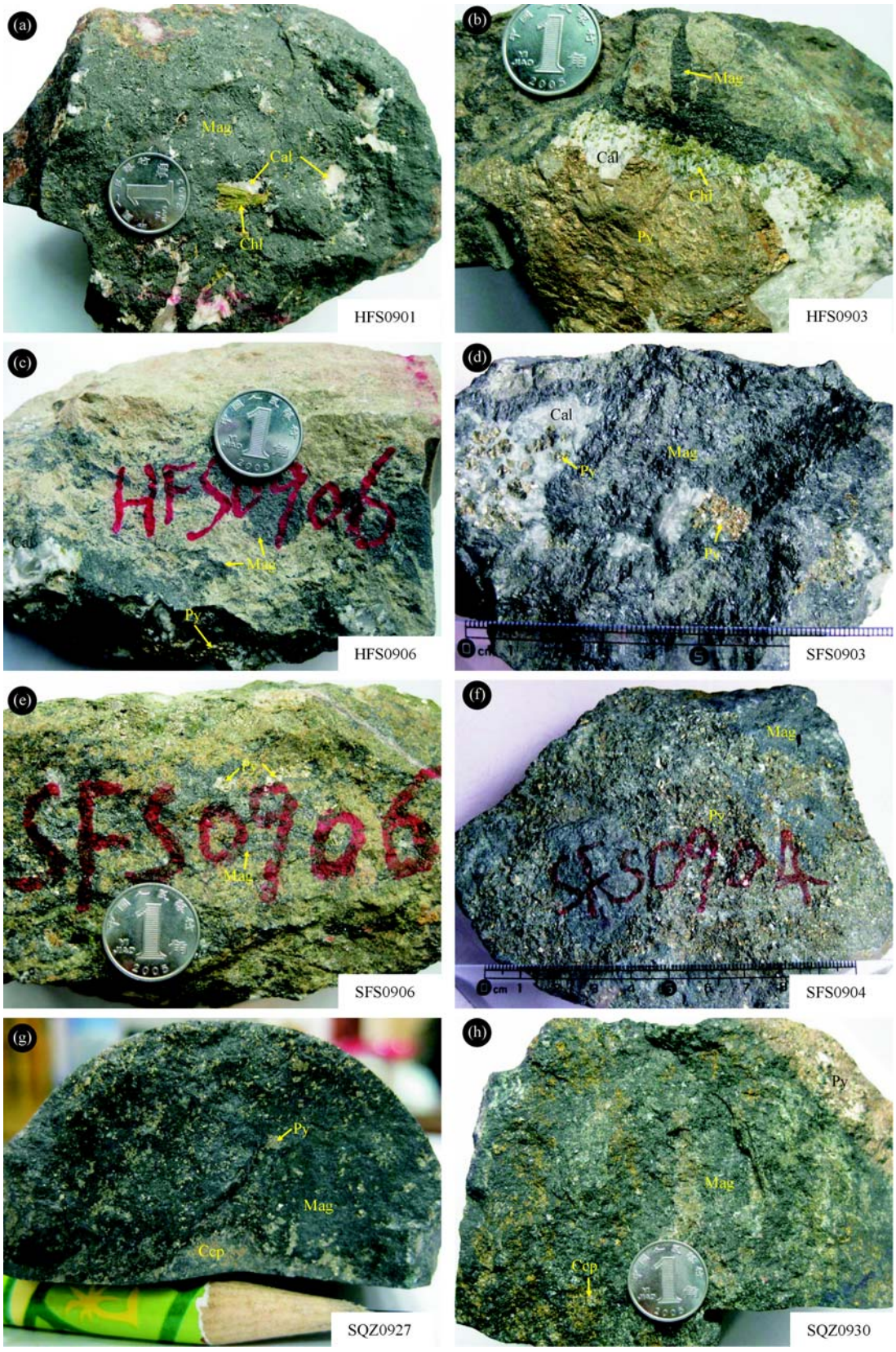

Fig. 3. Photos of ores from the Heifengshan, Shuangfengshan, and Shaquanzi Fe(–Cu) deposits in the Eastern Tianshan Orogenic Belt.
(a), Massive ore from the Heifengshan deposit with a mineral assemblage of magnetite, calcite, and chlorite; (b), Disseminated ore from the Heifengshan deposit composed of magnetite, pyrite, calcite, and chlorite; (c), Banded ore from the Heifengshan deposit consisting of magnetite, pyrite, and calcite; (d), Massive ore from the Shuangfengshan deposit with a mineral assemblage of magnetite, pyrite, and calcite; (e), Banded ore from the Shuangfengshan deposit consisting of magnetite and pyrite; (f), Massive ore from the Shuangfengshan deposit containing amounts of pyrite;. (f, g), Massive ore from the Shaquanzi deposit consisting of magnetite, pyrite, and chalcopyrite. Abbreviations: Mag, magnetite; Py, pyrite; Ccp, chalcopyrite; Cal, calcite; Chl, chlorite.

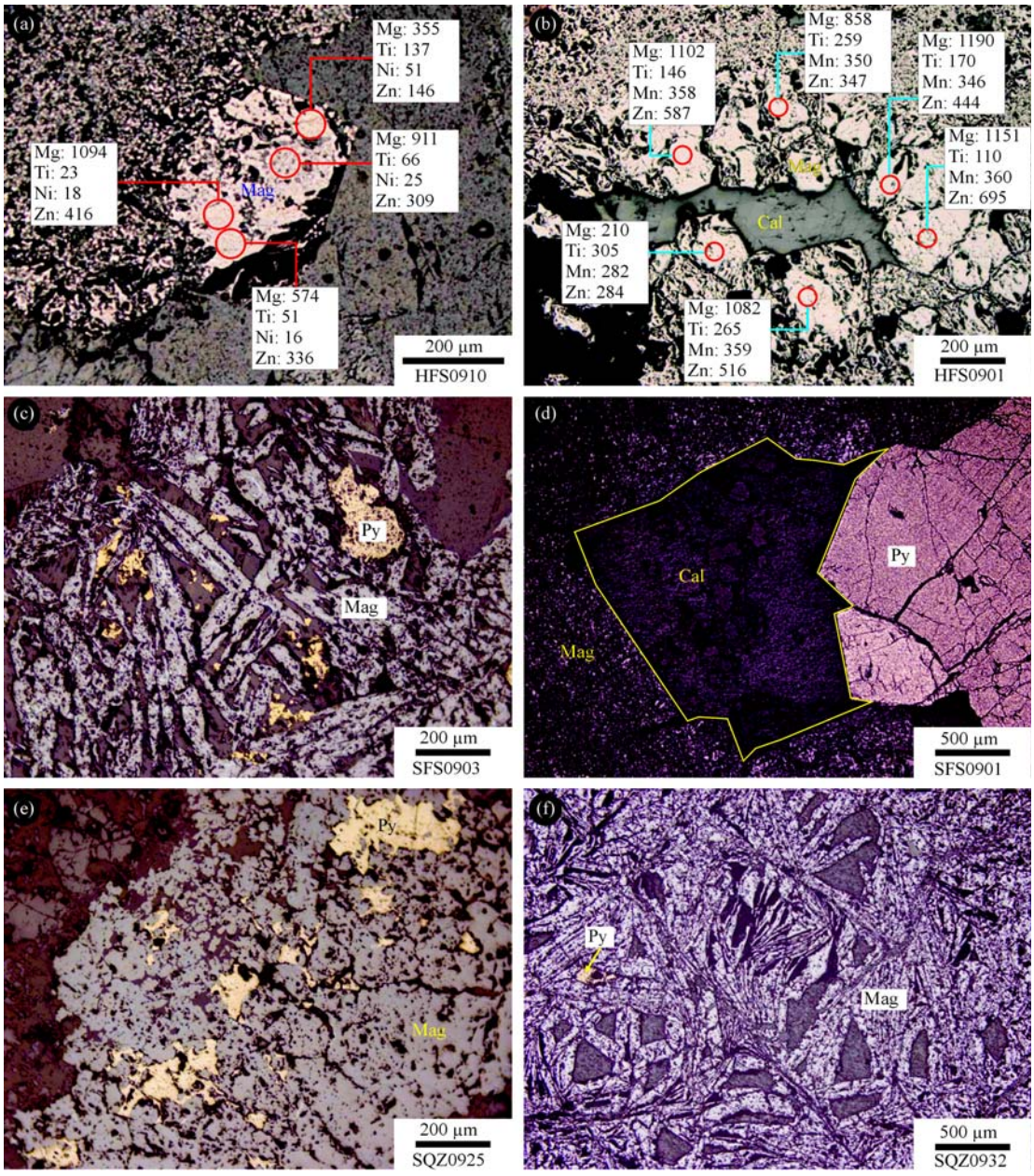

Fig. 4. Photomicrographs of ores from the Heifengshan, Shuangfengshan, and Shaquanzi Fe(–Cu) deposits in the Eastern Tianshan Orogenic Belt.

(a) The same magnetite grain has different Mg, Ti, Ni, and Zn concentrations (in ppm). (b) Different magnetite grains around the same calcite grain contain different Mg, Ti, Mn, and Zn. (c) Platy magnetite is associated with anhedral pyrite. (d) Clear contact boundaries among magnetite, pyrite, and calcite indicate mineral equilibrium. (e) Pyrite grows along the factures of magnetite. (f) Magnetite occurs as columnar or radial crystals and is locally infilled by pyrite. Abbreviations: Mag, magnetite; Py, pyrite; Cal, calcite.

Al, Ti, V, Cr, Mn, Co, Ni, Zn, and Ga in magnetite from these deposits are commonly 10 to 1000 times of their respective detection limits, whereas other elements are typically below or close to their respective detection limits and are not discussed later. Mean and stdev (standard deviation) values of selected elements for each sample are showed in Table 1 and detailed results of all analyses are given in Appendix.

Compositional variations between different magnetite grains from the same deposit typically do not exceed one order of magnitude. Magnetite from different deposits show different trace element patterns on the bulk continental crust normalized multi–element diagrams (Fig. 5). Magnetite from the Heifengshan Fe deposit is relatively rich in V and Zn but depleted in Cr (Fig. 5a), whereas those from the Shuangfengshan Fe deposit show relative enrichment of V, Mn and Zn but depletion of Cr and Ni (Fig. 5b). Most of the magnetite samples from the Shaquanzi Fe–Cu deposit display similar normalized trace element patterns with relative enrichment of V and Mn

Table 1 LA–ICP–MS results of selected trace element concentrations (in ppm) in magnetite from the Fe(-Cu) deposits, Eastern Tianshan Orogenic Belt, NW China

Sample no.		Mg	Al	Ti	V	Cr	Mn	Co	Ni	Zn	Ga
Detection limit		2.56	1.85	0.36	0.099	1.69	1.33	0.017	3.08	0.525	0.072
Heifengshan Fe deposit											
HFS0901	Average (n=16)	974	3178	239	80.9	2.19	353	25.1	34.3	428	13.0
	Stdev	291	589	101	17.2	3.00	29	3.2	12.9	161	3.3
HFS0903	Average (n=14)	725	3409	339	78.9	3.48	341	10.6	44.6	269	12.0
	Stdev	171	542	72.1	10.5	2.17	19	0.6	7.4	84	4.3
HFS0904	Average (n=13)	573	2932	463	97.9	4.85	366	8.50	57.4	172	11.5
	Stdev	415	902	143	18.6	1.72	40	0.74	8.4	140	4.1
HFS0906	Average (n=10)	640	2954	287	102	4.01	380	5.89	62.2	228	13.0
	Stdev	256	237	20.5	8	2.62	24	0.52	9.0	84	2.8
HFS0910	Average (n=13)	663	2788	214	61.9	2.65	352	16.9	37.7	288	13.4
	Stdev	336	898	118	19.0	3.00	42	1.3	13.5	146	1.6
Shuangfengshan Fe deposit											
SFS0901	Average (n=13)	1086	2615	167	23.9	3.15	1160	18.6	b.d.l.	636	6.21
	Stdev	550	422	72	4.5	1.32	446	6.8		206	0.50
SFS0902	Average (n=19)	758	2602	218	32.0	4.00	940	14.7	3.52	576	6.57
	Stdev	461	441	39	7.2	1.84	378	5.1	1.06	225	0.88
SFS0903	Average (n=18)	1196	2497	182	29.9	6.22	1447	23.2	b.d.l.	616	6.57
	Stdev	515	375	25	6.6	4.51	536	6.3		164	1.18
SFS0904	Average (n=17)	489	2895	231	26.6	12.4	579	6.78	4.36	366	9.82
	Stdev	293	609	57	8.5	14.5	94	2.34	2.50	175	1.97
SFS0905	Average (n=11)	346	2545	224	28.1	3.77	756	18.4	b.d.l.	375	7.23
	Stdev	146	436	63	13.6	1.90	70	3.7		166	2.07
SFS0906	Average (n=13)	311	2221	153	32.6	3.26	780	15.0	b.d.l.	425	4.48
	Stdev	338	425	66	6.2	2.04	133	2.8		166	1.36
SFS0910	Average (n=9)	391	2592	381	36.6	19.9	776	15.3	3.54	373	8.3
	Stdev	269	292	255	17.0	17.6	126	2.1	2.06	172	1.2
SFS0911	Average (n=14)	276	2493	215	24.4	3.39	784	25.8	b.d.l.	479	6.22
	Stdev	263	609	59	6.8	1.44	51	2.0		241	1.40
SFS0912	Average (n=2)	592	2232	375	75.6	4.37	770	15.4	3.75	376	6.65
	Stdev	553	915	228	41.4	1.42	12	1.6	0.35	182	0.87
Shaquanzi Fe–Cu deposit											
SQZ0917	Average (n=5)	99	835	168	4.51	6.20	749	15.6	b.d.l.	21.2	3.93
	Stdev	46	265	53	2.52	1.50	43	0.9		2.7	0.27
SQZ0922	Average (n=3)	33	348	161	106	42.5	798	2.35	8.42	43.5	2.77
	Stdev	10	51	54	20	28.4	146	0.13	4.25	15.1	0.23
SQZ0925	Average (n=3)	109	582	239	134	47.2	612	4.91	4.43	35.4	4.35
	Stdev	6	266	134	9	34.2	125	0.60	0.67	11.7	0.96
SQZ0927	Average (n=5)	81	358	174	94.6	12.6	596	7.19	5.54	28.6	3.53
	Stdev	68	183	70	22.0	7.6	78	0.96	2.68	8.3	0.76
SQZ0930	Average (n=2)	413	860	217	56.3	61.8	465	13.5	8.13	37.8	6.66
	Stdev	419	656	9	7.6	10.4	40	0.6	0.38	0.9	0.01
SQZ0932	Average (n=5)	93	420	278	150	15.1	336	8.18	7.32	21.7	14.2
	Stdev	72	132	42	19	13.4	36	4.26	3.25	1.7	0.9
SQZ0933	Average (n=1)	81	415	279	225	14.0	26	0.38	8.59	34.3	13.0

Notes: Detection limit = $3\times\sigma^{i}_{background}\times C^{i}_{RM}/cps^{i}_{RM}$, where $\sigma^{i}_{background}$ is the standard deviation of multiple determinations of element *i* in the background, C^{i}_{RM} and cps^{i}_{RM} are concentration and peak intensity of element *i* in the reference material, respectively. n = number of analyses. Stdev = standard deviation. b.d.l = below detection limit.

and depletion of Cr and Ni (Fig. 5c). Two samples, SQZ0917 and SQZ0933, have lower V, Mn and Co contents than others (Fig. 5c), which will be discussed in the later part.

To further highlight the compositional differences between different magnetite occurrences from the same deposit or between different magnetite grains from the same sample, binary plots of selected elements for all analyses are necessary. There are good correlations between Mg and Mn, Al and Ti, V and Ti for magnetite grains from the samples HFS0901 and HFS0904 (Fig. 6a, d, e). There is a weak correlation of Mg with Zn for magnetite grains from the samples HFS0904 and HFS0910 (Fig. 6b). Aluminum shows a good correlation with Ga for the samples HFS0901 and HFS0906 (Fig. 6c), and V correlates well with Ti for the sample HFS0903 (Fig. 6e). Vanadium also correlates with Ni for the sample HFS0904 (Fig. 6f). There are no correlations of V with Cr and Co with Ni for all the samples from the Heifengshan Fe deposit (Fig. 6g, h). There are no obvious differences of trace elements in magnetite between massive and disseminated ores except that the later has relatively limited variations of V and Ti contents (Fig. 6e). However, magnetite associated with pyrite commonly has lower Co contents than magnetite from the ores without pyrite (Fig. 6h). Compositional variations also exist within a single magnetite grain or between different grains from the same sample. For example, Mg, Ti, Mn, and Zn concentrations are inhomogeneous within one magnetite grain (Fig. 4a), whereas different magnetite grains around the calcite clots

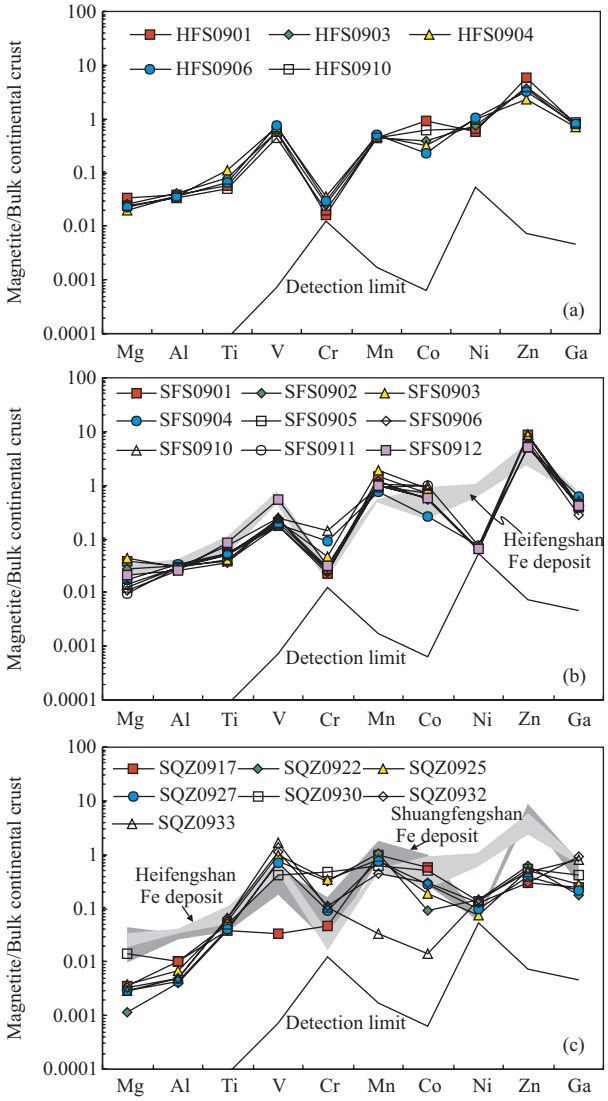

Fig. 5. Multi–element variation diagrams of median trace element concentrations in magnetite.
Normalized to bulk continental crust using values from Rudnick and Gao (2003).

have different Mg, Ti, Ni and Zn concentrations (Fig. 4b).

For the Shuangfengshan Fe deposit, inter–element correlations are not well–marked as those in the Heifengshan Fe deposit. Magnesium is correlated with Mn for the samples SFS0901 and SFS0903 (Fig. 7a). Magnesium also correlates with Zn for the samples SFS0901 and SFS0904 (Fig. 7b). Magnetite grains from the sample SFS0906 show a good correlation of V with Ti (Fig. 7c). Magnetite grains from the massive sulfide ore, SFS0904, have distinctly lower Mn and Co contents than others (Fig. 7a, d).

In the Shaquanzi Fe–Cu deposit, magnetite grains commonly contain abundant inclusions of silicates, resulting in the impurity of magnetite. The correlations between the selected elements are also not clear due to lack of enough data. There are some correlations of Mg with Al and V with Ti (Fig. 8a). The sample SQZ0917 is different from others by its low V contents (Fig. 8b), whereas the sample SQZ0933 has lower Mn and Co contents than other samples (Fig. 8c, d).

5.2 Factor analysis for trace elements in magnetite

The factor analysis for selected elements (Mg, Al, Ti, V, Mn, Co, Ni, Zn, Ga) have established three factors that account for over 75% of variability in the dataset (Fig. 9 and Table 2). Factors 1, 2 and 3 have element assemblages of Ni–Mn–V–Ti, Mg–Al–Zn and Ga–Co, respectively. To describe the factor scores of individual magnetite samples for the established factors, the factor scores (only outside the –0.5 to 0.5 intervals) are plotted in the X–Y space (Fig. 10). A greater score denotes a greater significance of the respective factor for the magnetite from the corresponding deposits. For example, magnetite from the Heifengshan Fe deposit has the largest scores for Factor 1 in the plots of Factor 1 versus Factor 3 but shows similar scores for Factor 1 with those from the Shuangfengshan Fe deposit in the plots of Factor 1 versus Factor 2, suggesting that magnetite from the Heifengshan Fe deposit cannot be identified by Factor 1 (Fig. 10). However, magnetite from the Shaquanzi Fe–Cu deposit has the largest overall scores for Factor 2 in Factor 2–Factor 3 space in spite of partial overlapping with magnetite from the Shuangfengshan Fe deposit in Factor 2–Factor 3 space, indicating that Factor 2 can be used to distinguish the Shaquanzi Fe–Cu deposit from the other two Fe deposits (Fig. 10).

6 Discussions

6.1 Compositional variations of magnetite

Trace element compositions of magnetite have shown that magnetite can accommodate a variety of trace elements into their crystal structures. But only spinel elements such as Mg, Al, Ti, V, Cr, Mn, Co, Ni, Zn and Ga are relatively enriched in magnetite because they can readily substitute Fe^{2+} or Fe^{3+} into magnetite spinel–type structure (Deer et al., 1992). Therefore, the subtle

Table 2 Rotated component matrix for the factor analysis of the selected elements

	Factor 1 (31.8%)	Factor 2 (23.4%)	Factor 3 (19.6%)
Ni	0.85	0.20	0.02
Mn	–0.76	0.41	–0.10
V	0.74	–0.22	–0.13
Ti	0.69	0.30	–0.19
Mg	–0.16	0.85	0.00
Al	0.31	0.80	0.12
Zn	–0.50	0.57	0.46
Ga	0.16	–0.08	0.93
Co	–0.36	0.26	0.78

Notes: Values in parentheses represent the variability the respective factors account for. Only factor scores outside –0.5 to 0.5 are considered to be important.

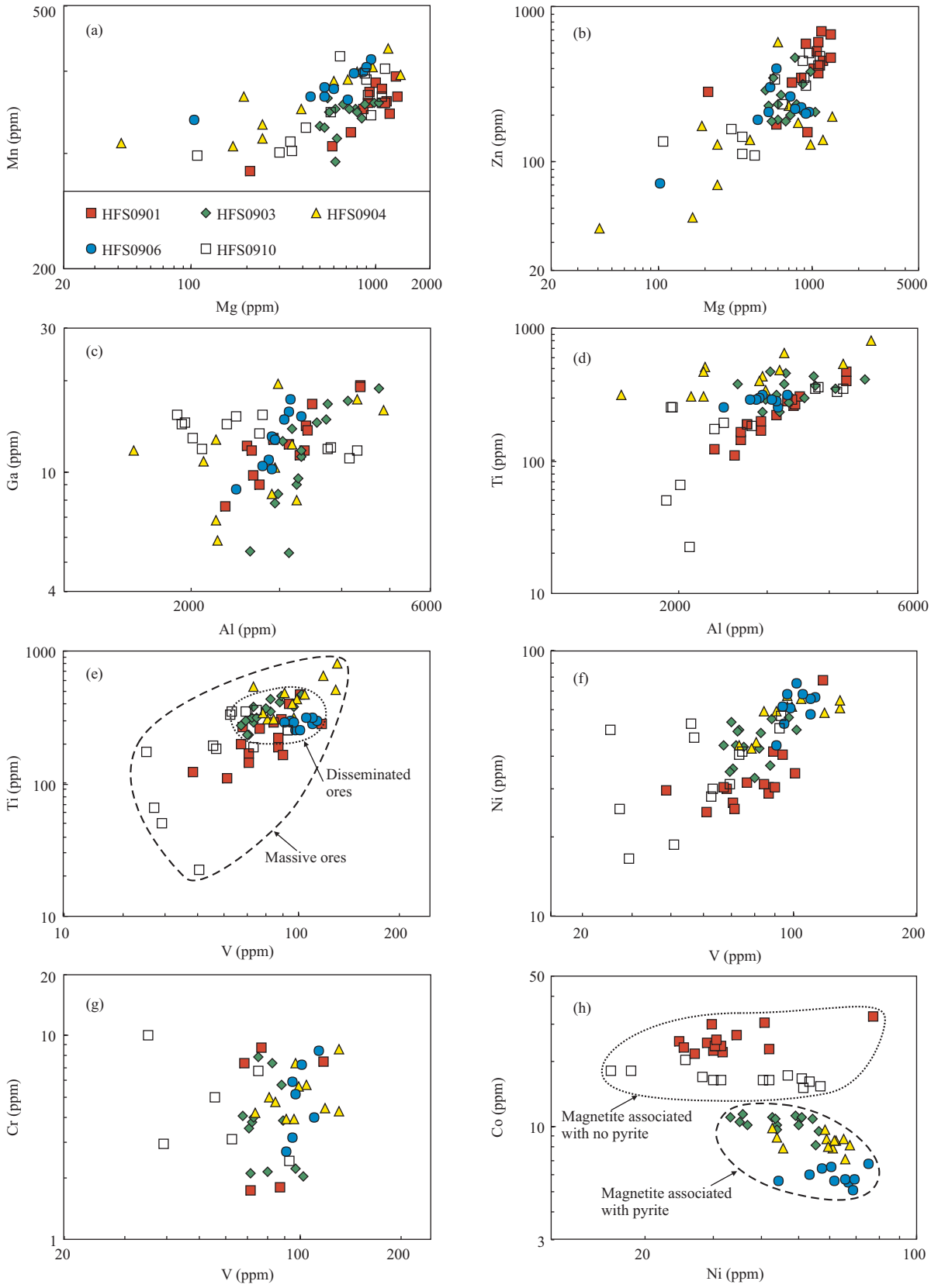

Fig. 6. Binary plots for the selected elements in magnetite from the Heifengshan Fe deposit.

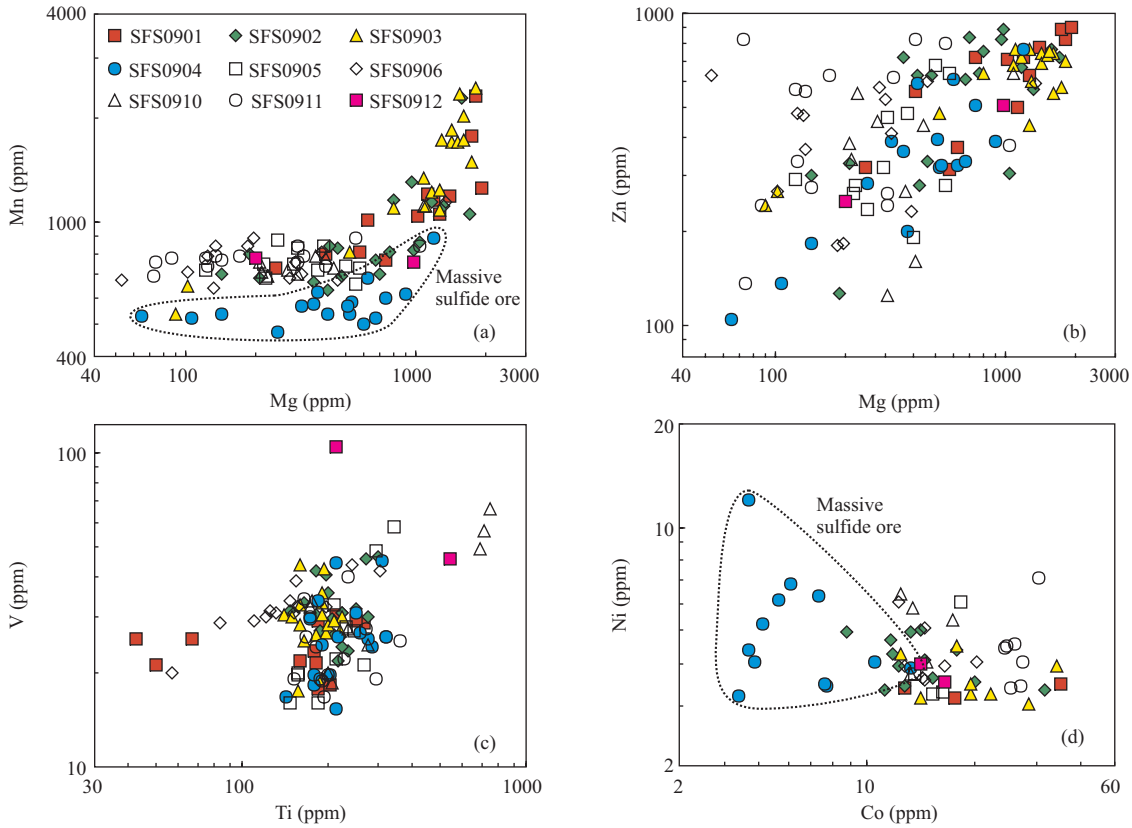

Fig. 7. Binary plots for the selected elements in magnetite from the Shuangfengshan Fe deposit.

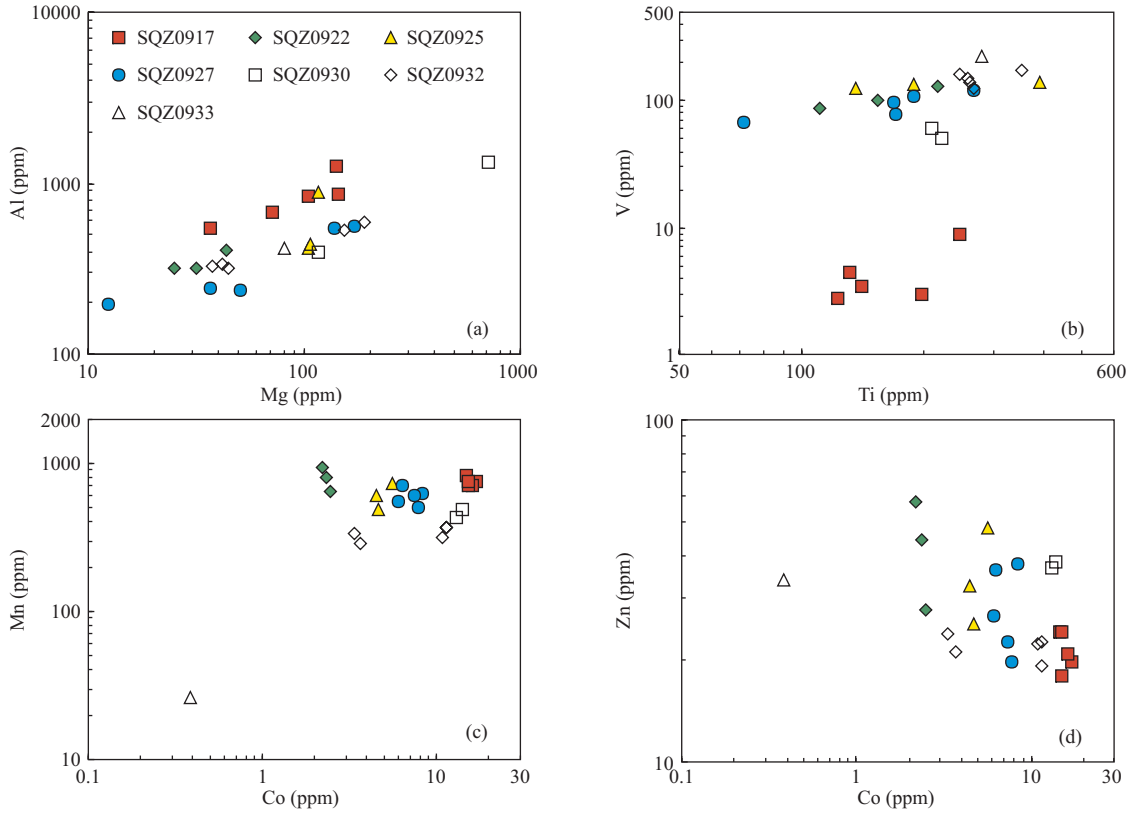

Fig. 8. Binary plots for the selected elements in magnetite from the Shaquanzi Fe–Cu deposit.

variations of these spinel elements can be used to distinguish magnetite from different sources (Carew, 2004; Rusk et al., 2009; Dupuis and Beaudoin, 2011) and indicate the physicochemical conditions for magnetite formation (Nadoll et al., 2012). As pointed out by Carew (2004), the compositional variations of magnetite can be controlled by numerous factors including host rock geochemistry, mineral assemblage, degree of fluid–rock interaction, and physicochemical conditions during deposition (e.g. P, T, pH, f_{O2} and f_{S2}).

6.1.1 Compositional variations within the same deposit

Five magnetite samples from the Heifengshan Fe deposit have similar normalized trace element patterns (Fig. 5a), indicating that they are derived from the same ore–forming fluids. However, the variable Mg, Ti, Ni and Zn concentrations within the same magnetite grain (Fig. 4b) and variable Mg, Ti, Mn and Zn contents between different magnetite grains within the same sample (Fig. 4b) indicate inhomogenous element distribution at a micrometer scale in magnetite. This variation may be related to the crystallization rate. The greater variations of V and Ti contents in magnetite from massive ores than from disseminated ores (Fig. 6e) may indicate different ore–forming conditions. Cobalt contents keep constant for individual magnetite samples (Fig. 6h), indicating that Co is well–distributed during fluid evolution. Magnetite associated with pyrite has obviously lower Co contents than those from the ores absent of pyrite (Fig. 6h), indicating that Co in magnetite is controlled by associated sulfides to some extent. However, there are no obvious differences in Ni contents between these two magnetite occurrences, indicating that associated pyrite has no significant effects on the Ni contents in magnetite. Carew (2004) also suggested that the presence or absence of pyrite in the same mineral assemblage has little effect on the amount of Ni in magnetite. Therefore, Ni in ore–forming fluids may partition into both magnetite and sulfides such as pyrite in equal amounts.

Similar to magnetite samples from the Heifengshan Fe deposit, those from the Shuangfengshan Fe deposit also have trace elements varying in a narrow range. Magnetite samples show identical bulk continental curst normalized trace element patterns except subtle variations of Cr contents (Fig. 5b), indicating the same sources of ore–forming fluids for magnetite precipitation. Magnetite grains from the massive sulfide ore, HFS0904, contain lower Mn and Co contents than those from other samples (Fig. 7a, d), which probably result from the different mineral assemblages. Larger proportion of pyrite in the massive sulfide ore (Fig. 3f) can be responsible for the lower Co contents in magnetite. However, similar Ni contents are identified in magnetite from both sulfide ores and other magnetite ores. Therefore, as demonstrated in the Heifengshan Fe deposit, Co rather than Ni in magnetite can be affected by the presence or absence of sulfides and the mineral proportion of sulfides.

Most magnetite samples from the Shaquanzi Fe deposit display similar normalized mean trace element patterns except two outliers of SQZ0917 and SQZ0933 (Fig. 5c). Magnetite grains from the sample SQZ0933 are commonly smaller than 30 μm across and are too small to analysis using beam spots of 44 or 60 μm. Due to limited data for the sample SQZ0933, the extremely low Mn and Co contents cannot be used to indicate the compositional variations among samples. The sample SQZ0917 has V content that is one order of magnitude lower than other samples (Fig. 8b). In many hydrothermal systems, the element V is essentially immobile in aqueous fluids (Goldshmidt, 1958) and is generally controlled by the composition of host rock and the degree of fluid–rock interaction (Carew, 2004). Considering ores from the Shaquanzi Fe deposit are hosted in the same strata, thus, the variation of V content may largely depends on the degree of fluid–rock interaction.

In summary, the ore–forming fluids responsible for the formation of Heifengshan, Shuangfengshan, and Shaquanzi Fe(–Cu) deposits are relatively uniform. The subtle variations of individual elements within a magnetite grain and between magnetite grains in the same sample are probably due to local fluid inhomogeneity, whereas large variations of Co in different magnetite samples may be largely related to the associated sulfides.

6.1.2 Compositional variations among deposits

The Heifengshan, Shuangfengshan, and Shaquanzi Fe(–Cu) deposits have similar mineral assemblages and hydrothermal alteration, but they have subtle differences in chemical compositions of magnetite. The sole difference of normalized trace element patterns between the Heifengshan and Shuangfengshan Fe deposits is the Ni content (Fig. 5b). As discussed above, Ni content in magnetite is controlled by both magnetite and pyrite. Considering that these two Fe deposits have similar trace element contents, we infer that the differences in Ni content is due to the different mineral proportions of magnetite and pyrite. Magnetite from the Shaquanzi Fe(–Cu) deposits contains lower Mg and Al but higher Zn than those from the Heifengshan and Shuangfengshan Fe deposits (Fig. 5c). Experimental studies have showed that Cu, Zn and Mn are preferably partitioned into the fluids with respect to Fe, and hence even minor to trace concentrations of these base metals in magnetite indicate strong enrichment of them in chloride–rich hydrothermal

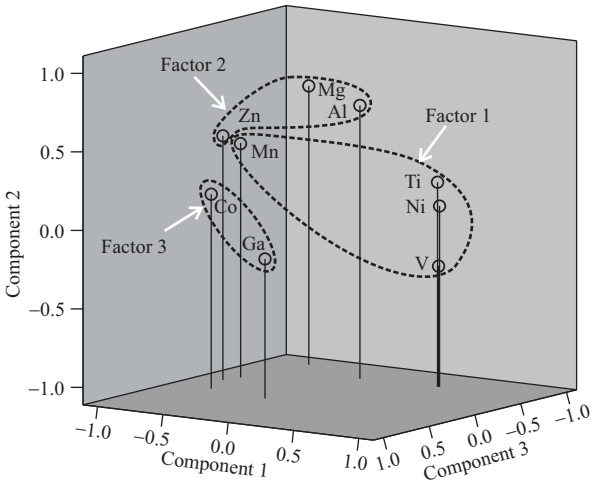

Fig. 9. Rotated component plot for magnetite from the Heifengshan, Shuangfengshan, and Shaquanzi Fe(–Cu) deposits in the Eastern Tianshan Orogenic Belt.
Factor 1 consists of Mn, Ti, Ni, and V. Factor 2 consists of Mg, Al, and Zn. Gallium and Co constitute the Factor 3. The lines project the position of the elements on the component 1– component 3 plane to show the importance of the elements for the components 1 and 3.

fluids (Ilton and Eugster, 1989). Therefore, relatively enriched Zn in magnetite from the Shaquanzi Fe–Cu deposit indicates that the ore–forming fluids are much richer in Zn.

Different origins of ore fluids for these Fe(–Cu) deposits can be identified by factor analysis. Trace elements of magnetite from the Fe(–Cu) deposits in the ETOB define three factors and the Shaquanzi Fe–Cu deposit shows affinity with Factor 2 (Mg, Al and Zn). This indicates that Fe–Cu ore system may be different from Fe ore system in the ETOB.

In summary, the Heifengshan and Shuangfengshan Fe deposits may be derived from the same ore–forming fluids. Ore–forming fluids responsible for the Shaquanzi Fe–Cu deposit are depleted in Mg and Al but rich in Zn relative to those Fe deposits.

6.2 Origin of magnetite

Types of magnetite can be discriminated by the trace element compositions of magnetite (Dupuis and Beaudoin, 2011). The magnetite from the Heifengshan, Shuangfengshan and Shaquanzi Fe(–Cu) deposits has low V, Ti and Cr contents (average 40 ppm, 170 ppm and 10 ppm, respectively; Table 1) similar to those from hydrothermal deposits (average 76 ppm, 1000 ppm and 57 ppm, respectively) but significantly lower than magmatic magnetite (average 1200 ppm, 1200 ppm and 1800 ppm, respectively) from the Mesoproterozoic Belt Supergroup (Nadoll et al., 2012). In the diagrams of Ca+Al+Mn verus

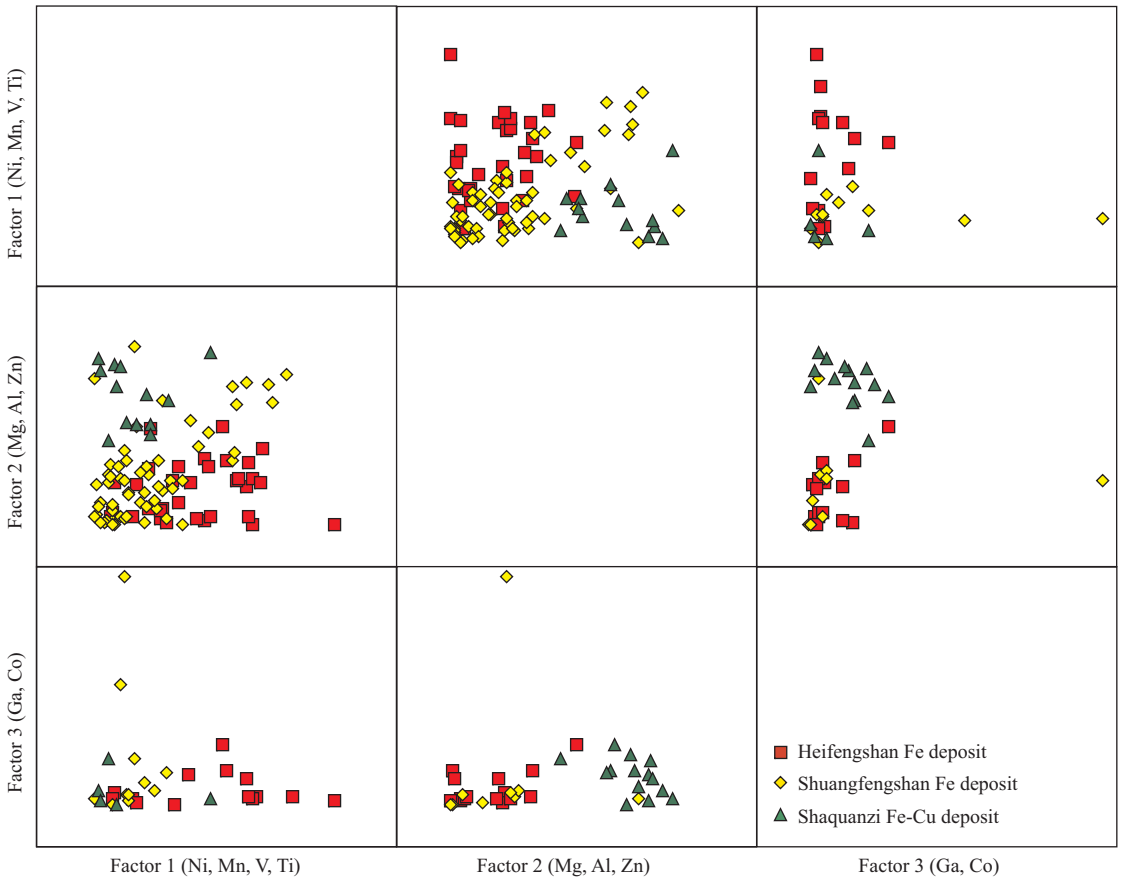

Fig. 10. Factor score plots for factors 1 to 3.

Ti+V (Fig. 11a) and Ni/(Cr+Mn) versus Ti+V (Fig. 11b), most magnetite grains plot in the "Skarn" field, indicating that magnetite from these Fe(–Cu) deposits may have formed by hydrothermal process rather than magmatic differentiation. The hydrothermal origin of magnetite from these deposits is consistent with the previous typomorphic study of magnetite (Li, 1985).

6.3 Comparison with magnetite from Banded Iron Formation (BIF) and Iron Oxide Copper Gold (IOCG) deposits

Although most magnetite grains from the Fe(–Cu) deposits plot in the "Skarn" field, minor magnetite grains also plot in the "BIF" and "IOCG" fields. To further illustrate the origin of magnetite, detailed comparison of trace elements between different types of deposits is very necessary. Magnetite from the Fe(–Cu) deposits in the ETOB has similar Mg, Al, Ti and Mn contents to those from the BIF, but the former has lower V, Cr, Ni and Zn contents than the latter (Fig. 12a). Moreover, much wider variations of V, Cr, Mn, Ni and Zn for magnetite from the Fe(–Cu) deposits than from the BIF. Magnetite from both the Fe(–Cu) deposits in the ETOB and IOCG deposits has a large variation of trace elements, indicating the complexity of ore–forming fluids. Magnesium, Al and Ti contents are indistinguishable for magnetite from the Fe(–Cu) deposits in the ETOB and IOCG deposits (Fig. 12b). However, magnetite from IOCG deposits is much richer in V, Cr, Ni, Mn and Zn than those from the Fe(-Cu) deposits in the ETOB (Fig. 12b). Therefore, magnetite from the Fe (–Cu) deposits in the ETOB has different origins compared to those from BIF and IOCG deposits in spite of their affinities.

6.4 Possible origin of Fe(-Cu) deposits in the ETOB

The origin of the Fe-(Cu) deposits in ETOB is still debated. These deposits were thought to be skarn type because of their close association with felsic intrusions (Song, 1985). They were also thought to be typical volcanic-hydrothermal deposits (Song et al., 1983), ore

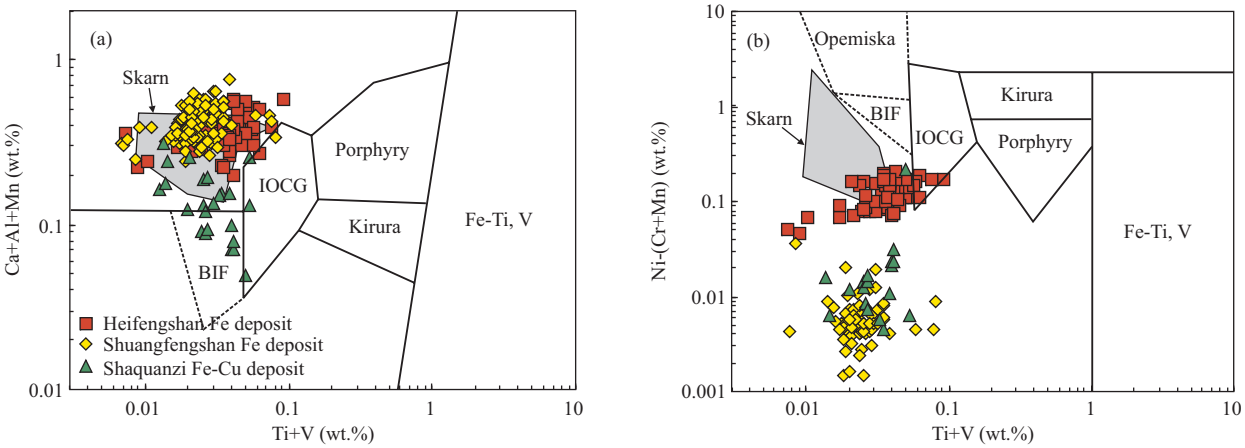

Fig. 11. Plots of Ca + Al + Mn vs. Ti + V (a) and Ni/(Cr + Mn) vs. Ti + V (b) for LA data of magnetite from the Heifengshan, Shuangfengshan, and Shaquanzi Fe(–Cu) deposits in the Eastern Tianshan Orogenic Belt.
The shaded areas represent the major range of skarn deposits. Reference fields are after Dupuis and Beaudoin (2011). BIF = banded iron formation, Skarn = Fe–Cu skarn deposits, IOCG = iron oxide–copper–gold deposits, Porphyry = porphyry Cu deposits, Kiruna = Kiruna apatite–magnetite deposits, Fe–Ti, V = magmatic Fe–Ti–oxide deposits.

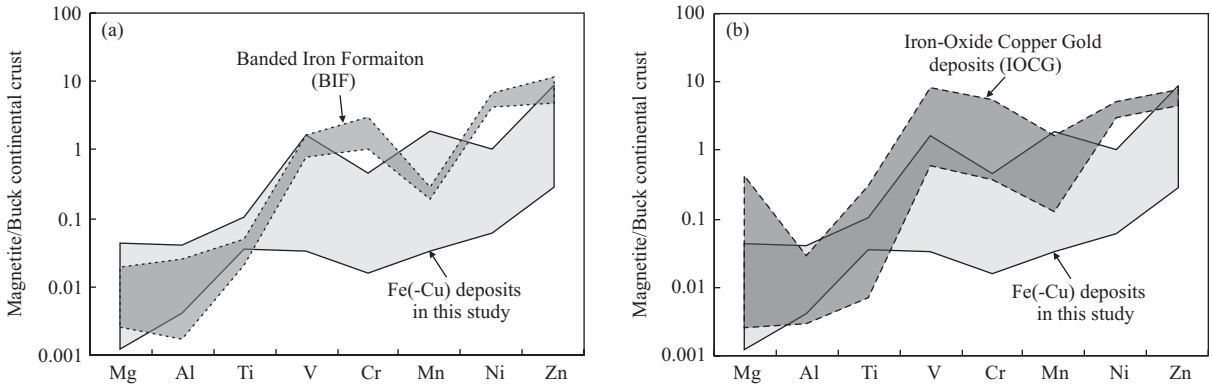

Fig. 12. Comparison diagrams of normalized trace element patterns for magnetite from Fe–(Cu) deposits in the Eastern Tianshan Orogenic Belt, Banded Iron Formation (BIF) and Iron–Oxide Copper Gold (IOCG) deposits.
Trace element contents of magnetite from BIF and IOCG deposits are from Dupuis and Beaudoin (2011). Normalized to bulk continental crust using values from Rudnick and Gao (2003).

slurry eruption–injection deposits (He et al., 1994a), contact metamorphic volcanogenic–sedimentary deposits (Jiang et al., 2002), and sedimentary exhalative deposits (SEDEX) (Wang et al., 2006b), because the Fe(–Cu) deposits are hosted in the strata of volcanic rocks or volcanoclastic rocks. Our detailed LA–ICP–MS study of magnetite provides important constrains on the origin of these Fe(–Cu) deposits.

As set forth, magnetite from the Heifengshan, Shuangfengshan, and Shaquanzi Fe(–Cu) deposits was derived from hydrothermal process rather than magmatic differentiation, and hence the possibility that magnetite was formed by ore slurry differentiated from late magma can be precluded. Magnetite from the Fe(–Cu) deposits shows skarn affinity in the plot of of Ca+Al+Mn vs. Ti+V (Fig. 11a), but they have lower Ni/(Cr+Mn) values than those from the skarn deposits (Fig. 11b). This indicates that these Fe(–Cu) deposits is closely related to skarn alteration but distinguish from skarn type deposits.

The Fe(–Cu) deposits are also not volcanogenic-sedimentary deposits because they have similar pyrite Re–Os ages of ~296 Ma that are obviously younger than the early to middle Carboniferous host volcanic rocks (Huang et al., 2013a). Their ores contain low-Ti magnetite (~150 to 460 ppm Ti, Table 1) and Fe/Cu–sulfides, different from SEDEX ores which are dominated by Fe/Cu–sulfides (Pirajno, 2009).

Pyrite from the Fe(–Cu) deposits has $\delta^{34}S_{CDT}$ values ranging from –0.41‰ to 4.7‰ (Huang et al., 2013a). Calcite from these deposits have similar C and O isotope compositions with $\delta^{13}C_{PDB}$ and $\delta^{18}O_{SMOW}$ ranging from –5.5‰ to –1.0‰ and from 10‰ to 12.7‰, respectively (Huang et al., 2013a). These stable isotopic data suggest that the ore–forming fluids are magmatic–hydrothermal in origin. Magnetite from these deposits has obviously lower contents of total trace contents (particularly V, Ti and Cr) than those from the Cihai Fe deposit in the Beishan terrane (Huang et al., 2013b). The elevated V, Ti and Cr contents are explained to be closely related to the hosting diabase (Huang et al., 2013b). Therefore, low trace element contents of magnetite indicate that the Fe(–Cu) deposits in the ETOB may be related to felsic magmatism.

7 Conclusions

(1) Laser ablation ICP–MS analyses show that magnetite from the Heifengshan, Shuangfengshan, and Shaquanzi Fe(-Cu) deposits in the ETOB contains detectable Mg, Al, Ti, V, Cr, Mn, Co, Ni, Zn, and Ga. The contents of these trace elements range from <0.01 to ~3000 ppm.

(2) Magnetite from the Shaquanzi Fe–Cu deposit contains lower Mg and Al but higher Zn than those from the Heifengshan and Shuangfengshan Fe deposits. The subtle variations of trace elements in magnetite can be used to discriminate different ore–forming fluids.

(3) The presence or absence of pyrite in the same mineral assemblage has little effect on the amount of Ni but has significant effect on the content of Co in magnetite.

(4) Low V and Ti contents in magnetite indicate that these deposits were probably derived from magmatic–hydrothermal fluids related to felsic magmatism.

Acknowledgements

This study was financially supported by the Chinese 973 project (2012CB416804), the ‘‘CAS Hundred Talents’’ Project from the Chinese Academy of Sciences (KZCX2-YW-BR-09) to Qi Liang. Field work was assisted by Deng Gang from No.6 Geological Team of Xinjiang and Gao Jianfeng from the Geological Survey of Canada. We also thank Gao Jianfeng and He Defeng for their assistance with LA-ICP-MS analyses. Two anonymous reviewers are thanked for their constructive suggestions that significantly improved the manuscript.

Manuscript received Jan. 26, 2013
accepted June 26, 2013
edited by Liu Lian and Hao Qingqing

Note

❶ Sinotech Minerals Exploration Co., Ltd., 2008. 1:1000000 geological map of mineral resources in eastern Tianshan.

❷ Bureau of Geology and Mineral Resources of Xinjiang Uygur Autonomous Region, 1965. 1:200000 geological map of Shaquanzi area numbered K–46–23.

References

Banvill, G., 1998. *Textural and geochemical investigation of the magnetite species at the Osborne Cu–Au deposit, Cloncurry District, Mount Isa Inlier, NW Queensland*. Townsville: James Cook University (Ph. D thesis).

Beaudoin, G., and Dupuis, C., 2009. Iron-oxide trace element fingerprinting of mineral deposit types. In: Corriveau, L., and Mumin, A.H. (eds.), *Exploring for iron oxide copper-gold deposits: Canada and global analogues*. GAC Short Course Notes, 107–121.

Berzina, A., 2012. Platinum-group element geochemistry of magnetite from porphyry-Cu-Mo deposits and their host rocks (Siberia, Russia). *Acta Geologica Sinica* (English Edition), 86 (1): 106–117.

Carew, M.J., 2004. *Controls on Cu–Au mineralisation and Fe oxide metasomatism in the Eastern Fold Belt, NW Queensland, Australia*. Queensland: James Cook University

(Ph. D thesis), 213–277.

Carew, M.J., Mark, G., Oliver, N.H.S., and Pearson, N., 2006. Trace element geochemistry of magnetite and pyrite in Fe oxide (+/–Cu–Au) mineralised systems: Insights into the geochemistry of ore-forming fluids. *Geochimica et Cosmochimica Acta*, 70(18): A83–A83.

Charvet, J., Shu Liangshu, Laurent-Charvet, S., Wang Bo, Faure, M., Cluzel, D., Chen Yan, and De Jong, K., 2011. Palaeozoic tectonic evolution of the Tianshan belt, NW China. *Science China Earth Sciences*, 54(2): 166–184.

Che Zicheng, Liu Honfu, and Liu Liang, 1994. *The formation of evolution of central Tianshan Orogenic Belt*. Beijing: Geological Publishing House (in Chinese).

Cliff, N., and Krus, D.J., 1976. Interpretation of canonical analysis: Rotated vs. unrotated solutions. *Psychometrika*, 41 (1): 35–42.

Dare, S.A.S., Barnes, S.J., and Beaudoin, G., 2012. Variation in trace element content of magnetite crystallized from a fractionating sulfide liquid, Sudbury, Canada: Implications for provenance discrimination. *Geochimica et Cosmochimica Acta*, 88: 27–50.

Davis, J.C., 1986. Statistics and data analysis in geology. 3rd ed. New York: John Wiley and Sons, Inc., 550.

Deer, W.A., Howie, R.A., and Zussman, J., 1992. *An introduction to the rock-forming minerals* (2nd ed). New York: Longman, Harlow, Wiley.

Devine, J.D., Rutherford, M.J., Norton, G.E., and Young, S.R., 2003. Magma storage region processes inferred from geochemistry of Fe-Ti oxides in andesitic magma, Soufriere Hills Volcano, Montserrat, WI. *Journal of Petrology*, 44(8): 1375–1400.

Dupuis, C., and Beaudoin, G., 2011. Discriminant diagrams for iron oxide trace element fingerprinting of mineral deposit types. *Mineralium Deposita*, 46(3): 1–17.

Fang Weixuan, Gao Zhenquan, Jia Runxin, Liu Zhentao, Li Fengshou, and Xu Guoduan, 2006a. Geological exploration potentials and geochemical study on rocks and ores in Shaquanzi copper and copper-iron deposits, east Xinjiang. *Acta Petrologica Sinica*, 22(5): 1413–1424 (in Chinese with English abstract).

Fang Weixuan, Huang Zhuanying, Tang Hongfeng, and Gao Zhenquan, 2006b. Lithofacies, geological and geochemical characteristics and tectonic setting of Late Carboniferous volcanic-sedimentary rocks in the Kumtag-Shaquanzi area, East Tianshan. *Chinese Geology*, 33(3): 529–544 (in Chinese with English abstract).

Frost, B.R., 1991. Stability of oxide minerals in metamorphic rocks. *Reviews in Mineralogy and Geochemistry*, 25(1): 469–488.

Gao Jun, Li Maosong, Xiao Xuchang, Tang Yaoqing, and He Guoqi, 1998. Paleozoic tectonic evolution of the Tianshan Orogen, northwestern China. *Tectonophysics*, 287(1–4): 213–231.

Gao Zhenjia, Chen Jibiao, and Lu Songnian, 1993. *Precambrian geology of northern Xinjiang*. Beijing: Geological Publishing House (in Chinese).

Goldshmidt, V.M., 1958. *Geochemistry*. London: Oxford University Press.

He Dalong, Zhou Jiyuan, and Mao Yanshi, 1994a. Occurrence and metallogenic mechanism of volcanic–type iron deposits in eastern Tianshan mountain. *Geological Sciences of Xinjiang*, 5: 41–53 (in Chinese with English abstract).

He Guoqi, Li Maosong, and Liu Dequan, 1994b. *Paleozoic crustal evolution and mineralization in Xinjiang of China*. Urimqi: Xinjiang People's Publishing House (in Chinese).

Hou Guangshun, Tang Hongfeng, and Liu Congqiang, 2006. Geochemical characteristics of Late Paleozoic volcanics in Jueluotage tectonic belt, eastern Tianshan and its implications. *Acta Petrologica Sinica*, 22(5): 1167–1177 (in Chinese with English abstract).

Hu Aiqin, Wei Gangjian, Zhang Jibin, Deng Wenfeng, and Chen Linli, 2007. SHRIMP U-Pb age for zircons of East Tianhu granitic gneiss and tectonic evolution significance from the eastern Tianshan Mountains, Xinjiang, China. *Acta Petrologica Sinica*, 23(8): 1795–1802 (in Chinese with English abstract).

Hua Linbao, 2001. Element geochemistry subarea and ore-finding direction of metallogenic district, Yamansu–Shaquanzi, eastern Tianshan, Xinjiang. *Journal of Guilin Institute of Technology*, 21(2): 99–103 (in Chinese with English abstract).

Hua Linbao, Yang Xiang, and Zhong Hua, 2002. Geochemical characteristics and ore-finding forecast of "shaquanzi" area, eastern Tianshan, Xinjiang. *Mineral Resources and Geology*, 16(5): 291–296 (in Chinese with English abstract).

Huang Xiaowen, Qi Liang, Gao Jianfeng, and Zhou Meifu, 2013a. First reliable Re-Os ages of pyrite and stable isotope compositions of Fe(-Cu) deposits in the Hami region, Eastern Tianshan Orogenic Belt, NW China. *Resource Geology*, 63(2): 166–187.

Huang Xiaowen, Zhou Meifu, Qi Liang, Gao Jianfeng, and Wang Yuwang, 2013b. Re-Os isotopic ages of pyrite and chemical composition of magnetite from the Cihai magmatic-hydrothermal Fe deposit, NW China. *Mineralium Deposita*, 48(8): 925–946.

Ilton, E.S., and Eugster, H.P., 1989. Base metal exchange between magnetite and a chloride-rich hydrothermal fluid. *Geochimica et Cosmochimica Acta*, 53(2): 291–301.

Jiang Fuzhi, Qin Kezhang, Fang Tonghui, and Wang Shulai, 2002. Types, geological characteristics, metallogenic regularity and exploration target of iron deposits in eastern Tianshan mountains. *Xinjiang Geology*, 20(4): 379–383 (in Chinese with English abstract).

Kaiser, H.F., 1958. The varimax criterion for analytic rotation in factor analysis. *Psychometrika*, 23(3): 187–200.

Li Wanmao, 1985. Typomorphic research of magnetite from the Fe deposits in the eastern Xinjiang. *Northwest Geology*(5): 1–5 (in Chinese).

Li Yuan, Yang Jinshui, Zhang Jian, Li Tianfu, Chen Songyong, Ren Yufeng, and Xu Xiangzhen, 2011. Tectonical significance of Carboniferous volcanics in eastern Tianshan. *Acta Petrologica Sinica*, 27(1): 193–209 (in Chinese with English abstract).

Liu Yongsheng, Hu Zhaochu, Gao Shan, Günther, D., Xu Juan, Gao Changgui, and Chen Haihong, 2008. In situ analysis of major and trace elements of anhydrous minerals by LA-ICP-MS without applying an internal standard. *Chemical Geology*, 257(1–2): 34–43.

Liu Shuwen, Guo Zhaojie, Zhang Zhicheng, Li Qiugen, and Zheng Haifei, 2004. Nature of the Precambrian metamorphic blocks in the eastern segment of Central Tianshan: Constraint from geochronology and Nd isotopic geochemistry. *Science in*

China Series D: Earth Sciences, 47(12): 1085–1094.

Müller, B., Axelsson, M.D., and Öhlander, B., 2003. Trace elements in magnetite from Kiruna, northern Sweden, as determined by LA–ICP–MS. *GFF*, 125(1): 1–5.

Mao Jingwen, Goldfarb, R.J., Wang Yitian, Hart, C.J., Wang Zhiliang, and Yang Jianmin, 2005. Late Paleozoic base and precious metal deposits, East Tianshan, Xinjiang, China: Characteristics and geodynamic setting. *Episodes*, 28(1): 23–30.

Mao Jingwen, Pirajno, F., Zhang Zuoheng, and Wan Yusheng, 2012. SHRIMP Zircon U–Pb Dating of Alkaline Dykes in the Pobei Area, Beishan Rift, Xinjiang Autonomous Region, China: Implications for Tectonic Setting and Mantle Plume Events. *Acta Geologica Sinica* (English Edition), 86(4): 879–884.

Nadoll, P., and Koenig, A.E., 2011. LA–ICP–MS of magnetite: methods and reference materials. *Journal of Analytical Atomic Spectrometry*, 26(9): 1872–1877.

Nadoll, P., Mauk, J.L., Hayes, T.S., Koenig, A.E., and Box, S.E., 2012. Geochemistry of magnetite from hydrothermal ore deposits and host rocks of the Mesoproterozoic Belt Supergroup, United States. *Economic Geology*, 107(6): 1275–1292.

Nielsen, R.L., Forsythe, L.M., Gallahan, W.E., and Fisk, M.R., 1994. Major–and trace–element magnetite–melt equilibria. *Chemical Geology*, 117(1): 167–191.

Norman, M.D., Pearson, N.J., Sharma, A., and Griffin, W.L., 1996. Quantitative analysis of trace elements in geological materials by laser ablation ICPMS: Instrumental operating conditions and calibration values of NIST glasses. *Geostandards and Geoanalytical Research*, 20(2): 247–261.

Nystroem, J.O., and Henriquez, F., 1994. Magmatic features of iron ores of the Kiruna type in Chile and Sweden; ore textures and magnetite geochemistry. *Economic Geology*, 89(4): 820–839.

Pirajno, F., 2009. *Hydrothermal processes and mineral systems*. London: Springer.

Qi Shijun, Wang Delin, and Liu Tong, 2008. Division of metalloigenetic region-zones and minerogenic features of major dominant mineral products in Xinjiang. *Xinjiang Geology*, 26(4): 348–355 (in Chinese with English abstract).

Qin Kezhang, Fang Tonghui, Wang Shulai, Zhu Baoqing, Feng Yimin, Yu Haifeng, and Xiu Qunye, 2002. Plate tectonics division, evolution and metallogenic settings in eastern Tianshan Mountains, NW China. *Xinjiang Geology*, 20(4): 302–308 (in Chinese with English abstract).

Qin Kezhang, Peng Xiaoming, San Jinzhu, Xu Xingwang, Fang Tonghui, Wang Shulai, and Yu Haifeng, 2003. Types of major ore deposits, division of metallogenic belts in eastern Tianshan, and discrimination of potential prospects of Cu, Au, Ni mineralization. *Xinjiang Geology*, 21(2): 143–150 (in Chinese with English abstract).

Rudnick, R.L., and Gao, S., 2003. Composition of the continental crust. in: Holland, H.D., and Turekian, K.K. (Eds.), *Treatise on geochemistry*. Oxford: Elsevier–Pergaman, 1–64.

Rusk, B.G., Oliver, N.H.S., Zhang, D., Brown, A., Lilly, R., and Jungmann, D., 2009. Compositions of magnetite and sulfides from barren and mineralized IOCG deposits in the eastern succession of the Mt Isa Inlier, *Australia Society for Geology Applied to Mineral Deposits, 10th Bi–ennial SGA Meeting*. Townsville, Australia, 656–658.

Ryabchikov, I.D., and Kogarko, L.N., 2006. Magnetite compositions and oxygen fugacities of the Khibina magmatic system. *Lithos*, 91(1): 35–45.

Shane, P., 1998. Correlation of rhyolitic pyroclastic eruptive units from the Taupo volcanic zone by Fe–Ti oxide compositional data. *Bulletin of Volcanology*, 60(3): 224–238.

Shi Yuruo, Liu Dunyi, Zhang Qi, Jian Ping, Zhang Fuqin, and Miao Laicheng, 2007. SHRIMP zircon U-Pb dating of the Gangou granitoids, Central Tianshan Mountains, Northwest China and tectonic significances. *Chinese Science Bulletin*, 52 (11): 1507–1516.

Singoyi, B., Danyushevsky, L., Davidson, G.J., Large, R., and Zaw, K., 2006. Determination of trace elements in magnetites from hydrothermal deposits using the LA ICP–MS technique. *SEG Keystone Conference*. Denver, USA: CD–ROM.

Song Zhijie, 1985. The formative conditions and mineralization of a group of magnetite deposits in volcanic –intrusive complex region near Hami, Xinjiang. *Bulletin of the Xi'an Institute of Geology and Mineral Resources, Chinese Academy of Geological Sciences*, 9: 58–73 (in Chinese with English abstract).

Song Zhijie, Ren Binchen, Wang Xinquan, Wei Shi'e, Yang Shuli, and Yao Ai'min, 1983. The metallogenesis of Yamansu, Heifengshan, Shaquanzi Fe deposits in the volcanic–intrusive complex area of the southern margin of the eastern section of north Tianshan, Xinjiang. *Annuals of Chinese Academy of Geological Sciences (Suppl)*: 114–115 (in Chinese).

Turner, M.B., Cronin, S.J., Smith, I.E., Stewart, R.B., and Neall, V.E., 2008. Eruption episodes and magma recharge events in andesitic systems: Mt Taranaki, New Zealand. *Journal of Volcanology and Geothermal Research*, 177(4): 1063–1076.

Wang Denghong, Li Chunjie, Chen Zhenghui, Chen Shiping, Xiao Keyan, Li Huaqin, and Liang Ting, 2006a. Metallogenic characteristics and direction in mineral research in east Tianshan, Xinjiang, China. *Geological Bulletin of China*, 25 (8): 910–915 (in Chinese with English abstract).

Wang Jinbin, Wang Yuwang, and He Zhijun, 2006b. Ore deposits as a guide to the tectonic evolution in the East Tianshan Mountains, NW China. *Geology in China*, 33(3): 461–469 (in Chinese with English abstract).

Xiao Wenjiao, Zhang Lianchang, Qin Kezhang, Sun Shu, and Li Jiliang, 2004. Paleozoic accretionary and collisional tectonics of the Eastern Tianshan (China): Implications for the continental growth of central Asia. *American Journal of Science*, 304(4): 370–395.

Xiao Yi, 2003. The geological characteristics and ore–finding oritention of Shaquanzi Cu deposit, Hami, Xinjiang. *Xinjiang Nonferrous Metals*, 26(2): 9–11 (in Chinese with English abstract).

Xu Xingwang, Ma Tianlin, Sun Liqian, and Cai Xinping, 2003. Characteristics and dynamic origin of the large–scale Jiaoluotage ductile compressional zone in the eastern Tianshan Mountains, China. *Journal of Structural Geology*, 25 (11): 1901–1915.

Yang Xingke, Tao Hongxiang, Luo Guichang, and Ji Jinsheng, 1996. Basic features of plate tectonics in east Tianshan of China. *Xinjiang Geology*, 14(3): 221–227 (in Chinese with English abstract).

Zeng Chuanli, 1962. Preliminary exploration report of the Shaquanzi Fe–Cu deposit, Hami, Xinjiang (in Chinese).

Zhang Dexian, Rusk, B., Oliver, N., and Dai Tagen, 2011. Trace element geochemistry of magnetite from the Ernest Henry IOCG Deposit, Australia. *11th biennial meeting SGA 2011–Let's talk ore deposits*. Antofagasta, Chile.

Zhang Dexian, Dai Tagen, and Hu Yi, 2012. Analysis of trace elements in magnetites using laser ablation–inductively coupled plasma–mass spectrometry. *Rock and Mineral Analysis*, 31(1): 120–126 (in Chinese with English abstract).

Zhang Lianchang, Xia Bin, Niu Hecai, Li Wenqian, Fang Weixuan, Tang Hongfeng, and Wan Bo, 2006. Metallogenic systems and belts developed on the Paleozoic continental margin in Xinjiang. *Acta Petrologica Sinica*, 22(5): 1387–1398 (in Chinese with English abstract).

About the first author

Huang Xiaowen, male; born in Jiangxi in 1985. He graduated from Institute of Geochemistry, Chinese Academy of Sciences as a Ph. D. on July in 2013, now he is an assistant researcher in Institute of Geochemistry, Chinese Academy of Sciences. His current interests include Re-Os geochronology of sulfides and ore genesis of hydrothermal Fe deposits. E-mail: huangxw507@gmail.com.

Appendix

LA-ICP-MS results of selected trace element concentrations (in ppm) for all spots of magnetite from the Fe(-Cu) deposits, Eastern Tianshan Orogenic Belt, NW China.

	Mg	Al	Ti	V	Cr	Mn	Co	Ni	Zn	Ga
Detection limit	2.56	1.85	0.36	0.099	1.69	1.33	0.017	3.08	0.525	0.072
Heifengshan Fe deposit										
HFS0901-S1	1151	2586	110	60.9	b.d.l	360	24.8	24.6	695	12.2
HFS0901-S2	1190	2926	170	70.9	1.75	346	21.7	26.8	444	12.9
HFS0901-S3	858	3404	259	76.6	8.70	350	22.1	31.9	347	14.3
HFS0901-S4	1102	2656	146	71.4	b.d.l	358	23.1	25.2	587	11.7
HFS0901-S5	1082	3426	265	68.4	7.39	359	22.6	30.1	516	13.8
HFS0901-S6	210	3495	305	88.8	b.d.l	282	22.9	41.8	284	16.8
HFS0901-S9	1013	2738	188	86.9	1.81	385	23.8	30.5	395	9.02
HFS0901-S10	1123	3369	288	84.3	b.d.l	357	23.7	31.6	417	11.8
HFS0901-S11	1089	3131	219	86.8	b.d.l	376	24.3	29.0	373	12.4
HFS0901-S12	580	4346	465	101	b.d.l	307	26.6	34.5	173	19.4
HFS0901-S13	911	2933	197	67.4	b.d.l	358	23.9	30.5	579	12.7
HFS0901-S14	929	4339	405	93.7	b.d.l	373	30.2	40.7	155	19.1
HFS0901-S18	1308	3302	284	118	7.50	392	32.3	77.5	655	11.3
HFS0901-S19	744	2353	122	48.5	b.d.l	322	29.7	29.8	326	7.64
HFS0901-S20	1320	2671	163	89.7	b.d.l	366	25.4	30.5	467	9.71
HFS0903-S1	603	3048	471	102	2.02	291	10.9	50.2	237	12.6
HFS0903-S2	850	3729	430	82.9	b.d.l	340	11.3	49.1	214	14.9
HFS0903-S3	501	4733	414	87.9	5.75	331	10.2	36.9	287	19.0
HFS0903-S5	986	4117	353	82.5	7.35	359	11.0	42.7	377	17.1
HFS0903-S6	779	3314	272	67.3	4.06	350	10.2	43.7	472	11.2
HFS0903-S7	719	3193	234	70.9	2.10	351	11.4	35.8	200	13.8
HFS0903-S8	563	2936	236	70.2	3.51	346	10.8	54.2	348	7.85
HFS0903-S12	526	2620	377	97.3	2.22	328	9.59	56.3	231	5.44
HFS0903-S13	603	2986	290	73.7	b.d.l	351	11.0	50.6	186	8.38
HFS0903-S14	879	3137	313	72.3	3.74	356	9.73	43.7	317	5.38
HFS0903-S15	797	3576	294	69.6	b.d.l	347	10.5	35.1	236	14.6
HFS0903-S16	670	3254	380	73.0	4.00	357	10.1	49.7	181	9.05
HFS0903-S17	1052	3758	366	80.3	2.14	358	11.1	33.2	210	16.8
HFS0903-S18	621	3322	310	75.3	7.83	316	10.8	43.5	269	11.7
HFS0904-S2	548	3286	460	88.6	3.84	365	8.18	55.3	182	9.48
HFS0904-S3	398	2118	307	81.1	5.00	350	7.96	45.3	138	10.9
HFS0904-S5	168	2257	506	130	8.55	307	7.90	60.7	44	5.89
HFS0904-S6	705	2247	473	105	5.73	389	7.04	65.7	227	6.84
HFS0904-S7	1179	2950	439	99.0	5.62	432	8.54	62.0	138	10.4
HFS0904-S8	976	3179	479	90.5	3.91	405	8.79	58.8	128	12.2
HFS0904-S9	803	4283	545	73.2	4.21	399	8.93	43.7	177	17.3
HFS0904-S10	598	4846	798	130	4.23	387	8.80	65.2	595	15.9
HFS0904-S11	1362	2908	406	96.3	3.87	395	8.22	67.5	195	8.44
HFS0904-S12	241	2993	339	78.6	b.d.l	317	9.79	42.8	129	19.6
HFS0904-S13	191	2251	306	84.7	4.76	366	8.02	59.3	171	12.8
HFS0904-S14	42	1540	317	96.4	7.32	312	8.68	61.2	37	11.7
HFS0904-S15	241	3253	650	119	4.40	331	9.65	58.0	70	7.99
HFS0906-S1	447	3166	256	98.1	b.d.l	365	6.51	60.6	185	17.3
HFS0906-S2	716	3136	279	111	3.97	361	6.44	57.3	260	15.9
HFS0906-S4	533	2902	296	114	8.43	366	5.51	67.0	304	13.1
HFS0906-S5	855	3069	289	94.7	5.96	398	5.99	53.2	222	14.9
HFS0906-S6	526	2941	311	110	b.d.l	378	5.66	65.5	207	12.8
HFS0906-S7	104	3312	314	105	b.d.l	338	5.10	69.0	72	15.2
HFS0906-S8	959	2906	297	94.4	3.16	417	5.61	61.3	211	10.2
HFS0906-S9	903	2863	288	91.1	2.71	405	5.62	44.2	206	10.9
HFS0906-S10	592	2463	251	101	7.19	376	6.76	75.2	398	8.75
HFS0906-S11	768	2781	291	96.6	5.19	398	5.65	69.0	219	10.4
HFS0910-S1	896	4144	334	62.5	3.09	388	17.1	28.3	350	11.1
HFS0910-S2	1136	4284	352	63.2	b.d.l	404	16.5	30.0	481	11.7
HFS0910-S3	880	3814	362	75.0	6.71	396	16.4	41.8	449	12.1
HFS0910-S4	649	3753	348	69.6	b.d.l	421	16.5	31.6	237	11.9
HFS0910-S5	423	2463	193	55.9	5.03	328	16.1	52.9	109	15.2
HFS0910-S6	348	2791	181	57.1	b.d.l	313	17.2	46.9	113	15.4
HFS0910-S7	574	1884	51	39.1	2.96	346	18.1	16.4	336	15.4
HFS0910-S8	1094	2104	23	50.5	b.d.l	365	18.1	18.5	416	11.8
HFS0910-S9	911	2022	66	37.1	b.d.l	368	20.2	25.4	309	13.0
HFS0910-S10	355	2367	173	35.3	10.0	302	16.6	50.6	146	14.4
HFS0910-S11	946	2750	190	73.3	b.d.l	344	16.5	40.4	500	13.3
HFS0910-S12	299	1944	252	93.0	b.d.l	302	15.5	56.5	164	14.6
HFS0910-S13	108	1929	256	92.8	2.44	297	15.1	51.0	136	14.4

Continued

Shuangfengshan Fe deposit										
SFS0901-S3	1807	2421	160	21.7	4.25	2324	34.9	3.48	821	5.64
SFS0901-S5	575	2042	42	25.5	3.25	813	11.5	b.d.l	316	7.11
SFS0901-S6	1135	2250	67	25.6	4.82	1198	19.1	b.d.l	496	6.41
SFS0901-S7	618	1908	50	21.2	3.70	1000	20.8	b.d.l	372	7.00
SFS0901-S12	740	2934	185	29.1	b.d.l	768	11.8	b.d.l	723	6.40
SFS0901-S15	1759	2645	178	23.3	2.30	1780	29.4	b.d.l	893	5.78
SFS0901-S16	1194	2595	214	30.4	3.66	1152	17.6	3.14	725	6.07
SFS0901-S17	1937	3501	270	28.6	b.d.l	1252	15.8	b.d.l	907	6.16
SFS0901-S18	245	2572	183	18.9	1.98	732	14.7	b.d.l	321	6.46
SFS0901-S19	409	2682	184	17.6	6.10	806	12.8	3.36	565	6.52
SFS0901-S20	1408	3029	251	29.2	2.85	1175	16.8	b.d.l	779	6.07
SFS0901-S21	1283	2867	203	18.4	2.21	1045	19.3	b.d.l	636	5.65
SFS0901-S22	1012	2544	183	21.4	2.36	1037	17.1	b.d.l	708	5.50
SFS0902-S2	212	3054	272	46.0	2.97	682	14.2	5.01	330	5.44
SFS0902-S3	417	2199	206	29.8	b.d.l	626	15.4	3.61	632	6.06
SFS0902-S4	703	2743	224	31.1	3.98	704	11.1	b.d.l	834	6.47
SFS0902-S5	188	2864	303	46.4	6.38	804	11.7	4.67	126	5.50
SFS0902-S6	144	2119	199	40.8	b.d.l	700	8.81	4.93	301	8.33
SFS0902-S7	481	2201	182	42.0	2.49	696	12.2	3.91	635	6.46
SFS0902-S8	1712	3783	280	29.9	5.56	1045	11.3	b.d.l	718	7.56
SFS0902-S9	1579	2647	226	30.9	2.25	2277	31.4	3.35	766	6.00
SFS0902-S10	1329	3069	236	23.5	2.85	1099	17.8	4.39	571	6.27
SFS0902-S11	953	2508	226	24.1	6.30	1308	17.9	b.d.l	820	6.08
SFS0902-S12	457	1995	148	31.4	6.08	830	11.8	4.24	333	6.56
SFS0902-S13	424	2177	183	30.7	2.05	842	10.8	b.d.l	278	8.23
SFS0902-S14	764	2367	199	35.6	7.21	813	13.2	b.d.l	646	6.60
SFS0902-S15	664	2657	220	26.0	3.12	772	11.2	3.32	613	5.07
SFS0902-S19	987	2621	211	26.5	5.34	822	12.7	3.44	883	6.44
SFS0902-S21	1173	2913	253	32.0	2.07	1141	20.1	3.53	670	6.75
SFS0902-S23	357	2234	166	33.2	5.67	663	13.2	4.96	719	6.32
SFS0902-S24	805	2334	189	27.2	3.43	1158	19.9	b.d.l	759	7.06
SFS0902-S25	1050	2945	216	21.8	4.98	870	14.6	4.08	306	7.65
SFS0903-S3	91	2073	157	17.6	6.94	535	21.0	b.d.l	243	7.38
SFS0903-S5	1178	2208	198	26.6	10.8	1223	20.8	b.d.l	720	4.93
SFS0903-S6	520	3034	186	19.1	4.42	814	14.1	3.18	479	6.19
SFS0903-S8	1282	2244	160	28.3	b.d.l	1235	19.6	3.25	766	4.70
SFS0903-S9	1426	2093	141	30.6	b.d.l	1709	26.1	b.d.l	746	5.76
SFS0903-S10	1441	2214	149	30.2	b.d.l	1836	24.4	b.d.l	688	5.77
SFS0903-S12	1837	2352	160	44.1	3.58	2429	34.1	3.90	697	7.03
SFS0903-S13	1092	2371	195	42.5	18.4	1339	22.2	3.26	685	5.96
SFS0903-S14	1099	2766	223	30.1	7.80	1111	16.1	b.d.l	763	6.01
SFS0903-S15	1626	2429	201	28.4	11.9	2015	28.7	3.02	748	5.14
SFS0903-S16	799	2306	181	26.4	6.18	1093	19.5	3.48	639	7.71
SFS0903-S18	1520	2395	192	33.5	2.88	1704	28.1	b.d.l	731	6.40
SFS0903-S19	1767	3245	190	30.3	5.50	1481	21.2	b.d.l	574	8.42
SFS0903-S20	1610	2819	191	35.9	5.89	1720	27.5	b.d.l	556	7.01
SFS0903-S21	1284	3267	211	29.1	6.47	1071	17.9	4.47	434	7.14
SFS0903-S23	102	2168	164	25.2	3.90	649	12.5	4.23	266	9.21
SFS0903-S24	1302	2557	222	27.0	8.87	1733	29.8	b.d.l	600	6.87
SFS0903-S25	1553	2411	161	32.9	7.49	2341	33.9	b.d.l	759	6.69
SFS0904-S1	519	3305	324	26.1	2.93	536	4.68	4.36	318	9.48
SFS0904-S4	250	2101	250	30.8	35.1	472	5.65	6.11	285	8.48
SFS0904-S6	322	2545	179	18.2	b.d.l	564	4.38	3.22	385	9.14
SFS0904-S7	378	3817	287	24.1	5.19	620	4.67	12.0	199	13.3
SFS0904-S8	413	2397	143	16.7	b.d.l	535	8.73	b.d.l	594	6.83
SFS0904-S9	142	2152	184	33.6	4.98	538	4.83	4.04	183	8.59
SFS0904-S10	525	3149	204	19.7	2.40	584	5.20	b.d.l	326	10.8
SFS0904-S11	903	4121	321	26.0	7.79	610	5.11	5.22	389	10.3
SFS0904-S14	597	2672	278	25.6	55.1	500	6.11	6.84	616	9.76
SFS0904-S15	1201	2963	216	25.9	7.76	889	13.3	3.87	765	6.58
SFS0904-S16	617	3707	309	45.1	10.9	679	10.5	4.05	324	11.1
SFS0904-S17	746	2861	180	19.7	12.5	600	6.51	b.d.l	507	9.87
SFS0904-S18	64	2450	216	45.0	13.3	529	5.90	b.d.l	104	7.03
SFS0904-S22	105	2336	191	24.5	15.6	521	7.74	3.44	136	13.6
SFS0904-S23	357	2527	173	29.4	2.12	576	7.13	b.d.l	361	10.6
SFS0904-S24	666	2627	262	26.9	28.2	523	7.58	3.49	334	10.8
SFS0904-S25	505	3489	215	15.3	5.16	569	7.34	6.29	394	10.6
SFS0905-S2	548	2637	234	27.8	b.d.l	656	15.3	b.d.l	282	10.3
SFS0905-S4	378	2767	157	20.0	5.38	720	13.7	3.71	475	7.34
SFS0905-S5	497	2931	250	27.1	2.55	741	15.2	3.25	683	5.67
SFS0905-S7	221	2569	147	16.1	2.19	687	16.2	b.d.l	280	9.08
SFS0905-S12	401	2346	345	57.9	2.10	849	21.5	b.d.l	191	4.81
SFS0905-S15	253	1994	297	48.6	6.80	883	26.3	b.d.l	235	6.49

Continued

SFS0905-S17	569	2391	156	19.7	4.15	732	21.9	b.d.l	637	7.27
SFS0905-S18	305	3376	185	16.0	6.18	835	17.7	b.d.l	461	8.02
SFS0905-S20	294	1832	210	32.6	4.66	753	19.4	b.d.l	319	3.86
SFS0905-S23	217	2323	216	22.1	3.99	747	18.5	6.05	263	6.53
SFS0905-S25	122	2828	270	21.1	2.91	717	16.5	3.31	294	10.2
SFS0906-S1	198	2960	306	41.9	3.81	888	14.3	b.d.l	181	3.40
SFS0906-S3	299	2953	243	43.9	2.02	758	13.2	b.d.l	529	4.71
SFS0906-S4	284	2127	126	31.3	2.90	679	14.5	5.10	580	5.00
SFS0906-S5	1363	2431	147	33.8	3.38	1135	20.5	4.00	598	6.74
SFS0906-S6	103	2169	131	30.9	b.d.l	706	12.8	3.93	268	5.09
SFS0906-S8	184	1688	57	20.0	3.27	845	14.4	3.61	180	2.22
SFS0906-S9	319	2218	199	32.4	b.d.l	700	13.6	b.d.l	414	6.02
SFS0906-S10	461	2105	111	29.1	2.84	671	12.2	6.06	609	5.45
SFS0906-S11	132	1688	155	39.0	b.d.l	641	13.2	b.d.l	469	4.58
SFS0906-S12	125	2116	122	30.0	8.42	789	21.2	b.d.l	477	5.49
SFS0906-S14	52	1812	156	32.5	5.02	676	14.5	3.56	629	3.73
SFS0906-S17	135	2660	153	31.0	4.23	848	16.7	3.93	363	3.38
SFS0906-S20	389	1950	84	28.7	3.56	807	14.7	b.d.l	231	2.47
SFS0910-S1	367	2752	693	49.2	12.8	790	14.7	b.d.l	267	8.94
SFS0910-S2	406	2556	716	56.6	28.6	783	13.3	3.72	159	9.58
SFS0910-S3	306	2304	746	66.7	5.08	703	12.4	6.40	124	6.86
SFS0910-S8	441	2175	177	33.8	8.31	725	16.1	b.d.l	435	7.71
SFS0910-S9	276	3050	201	20.0	8.07	724	17.2	b.d.l	450	10.1
SFS0910-S10	212	2718	209	18.4	6.6	714	18.3	b.d.l	341	9.11
SFS0910-S11	1073	2387	174	32.2	31.3	1099	17.3	5.33	645	7.44
SFS0910-S12	209	2928	276	24.6	19.3	758	14.8	4.02	385	7.98
SFS0910-S13	227	2456	237	27.5	59.2	689	13.4	5.78	552	6.79
SFS0911-S1	74	1686	230	22.0	b.d.l	764	27.3	4.04	135	3.09
SFS0911-S2	144	2599	202	19.6	6.64	772	24.7	4.51	277	8.97
SFS0911-S3	87	1855	296	19.0	3.13	784	27.5	b.d.l	242	4.38
SFS0911-S5	306	2456	274	27.4	4.92	755	23.1	b.d.l	265	6.84
SFS0911-S6	326	2864	194	16.8	3.57	790	23.8	b.d.l	623	7.26
SFS0911-S8	406	2307	151	19.1	b.d.l	739	25.3	3.40	826	5.16
SFS0911-S9	1045	4174	360	25.2	4.32	849	26.9	3.42	377	6.71
SFS0911-S11	136	2504	189	19.1	3.18	792	23.6	b.d.l	561	6.20
SFS0911-S13	307	1821	235	40.3	3.08	842	24.4	4.42	242	7.00
SFS0911-S14	123	2387	164	34.2	b.d.l	778	26.0	b.d.l	566	5.77
SFS0911-S16	72	2306	168	25.9	3.81	689	30.3	7.09	829	5.89
SFS0911-S17	170	2336	173	30.2	3.67	790	26.1	4.55	629	6.35
SFS0911-S18	548	2946	183	24.2	2.81	892	24.0	b.d.l	805	6.23
SFS0911-S19	125	2660	190	18.7	3.93	741	27.4	b.d.l	334	7.21
SFS0912-S12	201	1585	213	105	3.36	778	14.2	4.00	247	6.03
SFS0912-S16	983	2880	536	46.3	5.38	762	16.5	3.50	504	7.26
Shaquanzi Fe-Cu deposit										
SQZ0917-S1	37	543	123	2.8	6.56	819	14.8	b.d.l	23.9	4.28
SQZ0917-S2	144	867	141	3.4	8.52	751	17.0	4.73	19.6	3.79
SQZ0917-S7	71	677	248	8.9	6.14	712	16.1	b.d.l	20.7	3.61
SQZ0917-S8	103	840	198	3.0	4.69	716	15.1	b.d.l	17.9	4.13
SQZ0917-S11	141	1248	131	4.4	5.10	747	15.1	b.d.l	24.1	3.85
SQZ0922-S1	32	317	155	101	67.1	804	2.35	12.7	44.8	2.68
SQZ0922-S2	44	406	218	129	11.5	940	2.22	4.25	57.9	3.03
SQZ0922-S6	25	320	111	88.8	49.0	648	2.48	8.26	27.8	2.59
SQZ0925-S3	104	418	136	124	86.6	489	4.65	4.86	25.3	3.27
SQZ0925-S11	115	889	391	142	29.1	739	5.59	4.77	48.3	5.12
SQZ0925-S12	108	439	191	136	25.8	607	4.48	3.65	32.7	4.65
SQZ0927-S2	37	241	171	78.5	9.52	626	8.31	7.71	38.1	3.83
SQZ0927-S4	50	238	72	67.0	6.09	501	7.84	8.02	19.5	2.82
SQZ0927-S7	12	195	169	97.8	25.1	599	7.40	4.51	22.4	2.61
SQZ0927-S17	170	564	189	108	7.97	706	6.30	b.d.l	36.4	4.23
SQZ0927-S20	137	550	268	122	14.3	549	6.12	6.00	26.8	4.16
SQZ0930-S19	709	1323	211	61.7	54.5	493	13.9	7.86	38.4	6.67
SQZ0930-S20	117	396	223	50.9	69.2	437	13.0	8.40	37.1	6.65
SQZ0932-S8	189	598	263	139	30.6	287	3.67	6.71	21.0	14.7
SQZ0932-S13	41	337	269	125	4.53	337	3.37	7.88	23.7	14.0
SQZ0932-S15	44	316	259	151	28.5	313	10.8	8.01	22.2	14.6
SQZ0932-S19	152	525	352	174	8.55	372	11.5	b.d.l	22.5	15.0
SQZ0932-S20	38	325	249	161	3.24	369	11.5	11.5	19.2	12.8
SQZ0933-S11	81	415	279	225	14.0	25.9	0.38	8.59	34.3	13.0

Note: "-S1" represent the number of laser spots; b.d.l = below detection limit.